Part 1

Cosmological Weak Lensing and Large Scale Structure

Ludovic Van Waerbeke

Richard Massey

Cosmic Shear on Distant Galaxies

L. van Waerbeke[1,2] and Y. Mellier[1,3]

[1]Institut d'Astrophysique de Paris, 98 bis Bvd Arago, 75014, Paris, France

[2]University of British Columbia, Department of Physics & Astronomy, 6224 Agricultural Road, Vancouver, B.C. V6T 1Z1, Canada.

[3] Observatoire de Paris, LERMA, 77 Av. Denfert Rohcerau, 75014 Paris, France

Abstract. We review the scientific objectives and the present status cosmic shear studies. We discuss the future prospects and the role cosmic shear could play in a precision cosmology era.

1. Introduction

Gravitational deflection of light by large scale structures produces weak deformation on lensed galaxies that eventually modifies their ellipticity distribution. The statistical shape properties of the lensed galaxy population directly depend on the geometry of the universe and the properties of the (dark) matter density power spectrum. Weak lensing theory shows this cosmological information can be derived from the observation of a large sample of distant galaxies of cosmic shear surveys.

Although it is believed cosmic shear surveys provide an unbiased view of the matter distribution in the Universe, gravitational distortion is a weak signal that turns out be difficult to measure and not easy to interpret from a cosmological point of view. As its amplitude increases as angular scale decreases, it is primarily sensitive to non-linear power spectrum predictions. Furthermore, in the weak lensing regime, ellipticity of galaxies produced by gravitational lensing is much weaker than other systematic effects, making the Point Spread Function corrections a most challenging issue.

This review gives a present day picture of cosmic shear research. We focus on observations, data analysis and related cosmological interpretations and discuss the technical issues and next challenges. By *cosmic shear*, we mean distortion of the distant galaxies only. The magnification aspects of gravitational lensing by large scale structures, or weak lensing on CMB anisotropy will not be reviewed.

## 2. Description of large scale structures with weak lensing

2.1. *Light propagation in the inhomogeneous universe*

The metric of the homogeneous Universe is written in the form (Schneider *et al.* 1998):

$$ds^2 = c^2\,dt^2 - a^2(t)\left[dw^2 + f_K^2(w)d\omega^2\right]\ , \qquad (2.1)$$

where $a(t) = (1+z)^{-1}$ is the cosmic scale factor normalized to unity today, $w(z)$ is the radial coordinate, and $f_K(w)$ is the comoving angular diameter distance out to a radial distance $w(z)$:

$$w(z) = \int_0^z dz'\,\frac{c}{H} = \frac{c}{H_0}\int_0^z \frac{dz'}{\sqrt{(1+z')^3\Omega_0 + (1+z')^2(1-\Omega_0-\Omega_\Lambda) + \Omega_\Lambda}}\ , \qquad (2.2)$$
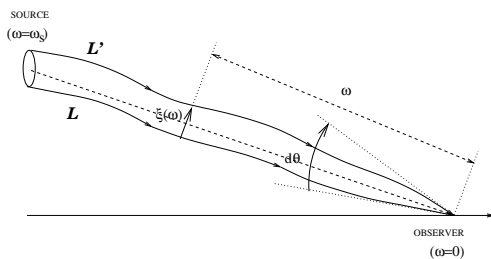
Figure 1. A light bundle and two of its rays $\mathcal{L}$ and $\mathcal{L}'$. $\boldsymbol{\xi}(w)$ is the physical diameter distance, which separates the two rays on the sky, viewed from the observer ($w = 0$).

where H_0 is today's Hubble constant, and the angular diameter distance $f_K(w)$ reads

$$f_K(w) = \begin{cases} K^{-1/2} \sin(\sqrt{K}w) & \text{for } K > 0 \,, \\ w & \text{for } K = 0 \,, \\ (-K)^{-1/2} \sinh(\sqrt{-K}w) & \text{for } K < 0 \,, \end{cases} \tag{2.3}$$

where K is the curvature

$$K = \left(\frac{H_0}{c}^2\right)(\Omega_0 + \Omega_\Lambda - 1) \,, \tag{2.4}$$

with Ω_0 and Ω_Λ the mean density parameter and the vacuum energy today.

Consider two light rays $\mathcal{L}$ and $\mathcal{L}'$ coming from a distant source and converging to an observer, and define $\mathrm{d}\boldsymbol{\theta}$ as the observed angular vector between the two rays (Figure1). We use the Cartesian complex coordinates, so $\mathrm{d}\boldsymbol{\theta} = (\mathrm{d}\theta_1, i\mathrm{d}\theta_2)$. In the absence of any inhomogeneities along the line of sight, the physical distance between the two rays at an angular distance $f_K(w_S)$ from the observer to the source is defined as $\boldsymbol{\xi} = f_K(w_S)\,\mathrm{d}\boldsymbol{\theta}$. Due to the inhomogeneities, the physical distance $\boldsymbol{\xi}$ deviates from this relation, and can be linearized as:

$$\begin{aligned} \boldsymbol{\xi} = f_K(w_S)\mathcal{A}\,\mathrm{d}\boldsymbol{\theta} &= f_K(w_S) \begin{pmatrix} \kappa + \gamma & -i\omega \\ -i\omega & \kappa - \gamma \end{pmatrix} \mathrm{d}\boldsymbol{\theta} \\ &= f_K(w_S)(\kappa - i\omega)\,\mathrm{d}\boldsymbol{\theta} + f_K(w_S)\gamma\,\mathrm{d}\boldsymbol{\theta}^\star. \end{aligned} \tag{2.5}$$

where $\mathcal{A}$ is by definition the amplification matrix. The description of an infinitesimal relative displacement of two rays $\mathcal{L}$ and $\mathcal{L}'$ is given by the quantities

$$\mathrm{d}\boldsymbol{\xi}_\kappa \propto \begin{pmatrix} \kappa\,\mathrm{d}\theta_1 \\ i\kappa\,\mathrm{d}\theta_2 \end{pmatrix}; \; \mathrm{d}\boldsymbol{\xi}_\gamma \propto \begin{pmatrix} \gamma\,\mathrm{d}\theta_1 \\ -i\gamma\,\mathrm{d}\theta_2 \end{pmatrix}; \; \mathrm{d}\boldsymbol{\xi}_\omega \propto \begin{pmatrix} \omega\,\mathrm{d}\theta_2 \\ -i\omega\,\mathrm{d}\theta_1 \end{pmatrix} \tag{2.6}$$

which contain the cosmological information. κ, γ and ω are called the convergence, the shear and the rotation fields, respectively. When the shear is not expressed in the eigenspace, $\boldsymbol{\gamma}$ is a complex vector in general (see Figure 2).

A light beam is a congruence of null geodesics, which are marked with respect to a fiducial geodesic having a tangent vector k_μ. The rays $\mathcal{L}$ and $\mathcal{L}'$ are two geodesics of the congruence, whose the separation $\boldsymbol{\xi} = \xi_1 + i\xi_2$ is defined as a space-like vector perpendicular to the wave-vector k_μ. For an infinitesimal displacement along the congruence it is always possible to decompose the geometrical deformation of the ray bundle into a uniform expansion Θ, a shear σ and a rotation W. This defines the optic scalars (Sachs 1961):

$$\frac{d(\Theta + iW)}{d\lambda} + (\Theta + iW)^2 + |\sigma|^2 = \mathcal{R} = \frac{1}{2}R_{\mu\nu}k^\mu k^\nu$$

$$\frac{d\sigma}{d\lambda} + \sigma\Theta = \mathcal{F} = C_{\mu\alpha\nu\beta}k^{\mu}k^{\nu}\bar{t}^{\alpha}\bar{t}^{\beta}. \tag{2.7}$$

Here, the geodesic is parametrized with $d\lambda = dw/(1+z)^2$. $R_{\mu\nu}$ and $C_{\mu\alpha\nu\beta}$ are the Ricci and the Weyl tensors respectively. t^{α} is the complex null tetrad (or Sachs tetrad) such that $t^{\alpha}k_{\alpha} = 0$ and $\bar{t}_{\alpha}t^{\alpha} = 1$. The first equation in (2.7) is the Raychaudhuri equation for null geodesics.

For an infinitesimal displacement along the congruence, the separation $\boldsymbol{\xi}$ transforms according to Eq.(2.5):

$$\frac{d\boldsymbol{\xi}}{d\lambda} = (\Theta - iW)\boldsymbol{\xi} + \sigma\boldsymbol{\xi}^{\star}. \tag{2.8}$$

Differentiating Eq.(2.8) and substituting Eq.(2.7) leads to the evolution equation of $\boldsymbol{\xi}$ along the congruence as a function of the gravitational fields $\mathcal{R}$ and $\mathcal{F}$:

$$\frac{d^2\boldsymbol{\xi}}{d\lambda^2} = \begin{pmatrix} \mathcal{R} - Re(\mathcal{F}) & iIm(\mathcal{F}) \\ iIm(\mathcal{F}) & \mathcal{R} + Re(\mathcal{F}) \end{pmatrix}\boldsymbol{\xi}. \tag{2.9}$$

For a Newtonian gravitational potential, Φ, $\mathcal{R}$ and $\mathcal{F}$ write:

$$\mathcal{R} = -\frac{1}{a^2(w)}\Delta\Phi \; ; \quad \mathcal{F} = -\frac{1}{a^2(w)}(\partial_1^2\Phi - \partial_2^2\Phi + 2i\partial_1\partial_2\Phi), \tag{2.10}$$

where $a(w)$ is the scale factor of the unperturbed background metric, and w the radial distance. Using a perturbative expansion for the amplification matrix $\mathcal{A}_{ij} = \mathcal{A}_{ij}^{(0)} + \mathcal{A}_{ij}^{(1)} + ...$ and for the gravitational potential $\Phi = \Phi^{(1)} + \Phi^{(2)} + ...$, Eq.(2.9) can be solved iteratively. The homogeneous universe case corresponds to $\mathcal{A}_{ij} = \mathcal{A}_{ij}^{(0)} = \delta_{ij}$ and $\Phi = 0$. It is then easy to obtain the general first order solution for the amplification matrix in the direction $\boldsymbol{\theta}$:

$$\mathcal{A}_{ij}(\boldsymbol{\theta}) = \delta_{ij} + \mathcal{A}_{ij}^{(1)}(\boldsymbol{\theta}) = \delta_{ij} - \frac{2}{c^2}\int_0^{w_S} dw \; \frac{f_K(w-w')f_K(w')}{f_K(w)}\Phi_{,ij}^{(1)}(f_K(w')\boldsymbol{\theta}, w'), \tag{2.11}$$

where w_S is the position of the source. Eq.(2.11) is the basic lensing equation used to calculate the distortion and the magnification of distant sources. This result is a first order expression and is only valid in the realm of the Born approximation where the lensing properties are calculated along the unperturbed light path (of direction $\boldsymbol{\theta}$). Therefore, all contribution coming from the lens-lens coupling are neglected (for most practical applications this is indeed an excellent approximation).

Back to the lensing effects (Eq.2.5), the geometrical deformation of a light bundle can be expressed as an integrated effect along the line-of-sight:

$$\kappa = 1 + \frac{1}{2}Tr(\mathcal{A}_{ij}^{(1)}) \; ; \quad \gamma = \frac{1}{2}(\mathcal{A}_{11}^{(1)} - \mathcal{A}_{22}^{(1)} + 2i\mathcal{A}_{12}^{(1)}) \; ; \quad \omega = 0. \tag{2.12}$$

These expressions show that, to first order ($\omega = 0$), a scalar perturbation does not induce a rotation of the light bundle. Figure 2 shows the effect of cosmic shear on a distant circular galaxy, in the weak lensing regime ($\kappa \ll 1$ and $\gamma \ll 1$). It shows that the shear can be obtained from the measurement of the shape of galaxies.

2.2. Mean fields

The second order derivatives of the gravitational potential field can be written as function of the mass density contrast δ, using the Poisson equation:

$$\nabla^2\Phi = \frac{3H_0^2\Omega_0}{2a}\delta. \tag{2.13}$$
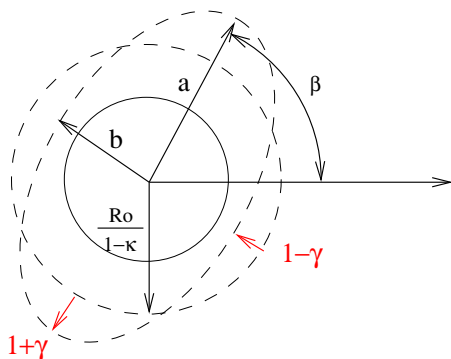
Figure 2. Illustration of the first order effect of cosmic shear on a circular background galaxy of radius R_0. The convergence is an isotropic distortion of the image of the galaxy, while the shear is an anisotropic distortion.

From Eq(2.11), we get the convergence $\kappa(\boldsymbol{\theta})$ in the direction $\boldsymbol{\theta}$, as function of δ, integrated along the line of sight:

$$\kappa(\boldsymbol{\theta}, w) = \frac{3}{2} \frac{H_0^2}{c} \Omega_0 \int_0^{w_S} \mathrm{d}w' \, \frac{f_K(w - w') \, f_K(w')}{f_K(w)} \frac{\delta\left(f_K(w')\boldsymbol{\theta}, w'\right)}{a(w')}, \qquad (2.14)$$

with similar (but not identical) expressions for $\boldsymbol{\gamma}(\boldsymbol{\theta})$. The sources have been assumed to be at a single 'redshift' w_S. For a more realistic redshift distribution, the lensing fields are integrated along the redshift with the proper source distribution $p_w(w)\mathrm{d}w$ from 0 to the horizon w_H:

$$\kappa(\boldsymbol{\theta}) = \frac{3}{2} \left(\frac{H_0}{c}\right)^2 \Omega_0 \int_0^{w_\mathrm{H}} \mathrm{d}w \, g(w) \, f_K(w) \frac{\delta\left(f_K(w)\boldsymbol{\theta}, w\right)}{a(w)}, \qquad (2.15)$$

with

$$g(w) = \int_w^{w_\mathrm{H}} \mathrm{d}w' \, p_w(w') \frac{f_K(w' - w)}{f_K(w')}. \qquad (2.16)$$

2.3. Limber equation and small angle approximation

The statistical properties of the lensing fields are given by the moments of the field. The variance is the first non trivial moment; its evolution with angular scale depends on cosmological parameters and on the geometrical properties of the Universe due to the light rays propagation. The mass density power spectrum $P_{3D}(k)$ is defined as

$$\langle \tilde{\delta}(\mathbf{k})\tilde{\delta}^*(\mathbf{k}') \rangle = (2\pi)^3 \delta_\mathrm{D}(\mathbf{k} - \mathbf{k}') \, P_{3D}(k, w). \qquad (2.17)$$

Likewise, one can define the convergence power spectrum $P_\kappa(s)$:

$$\langle \tilde{\kappa}(\mathbf{s})\tilde{\kappa}^*(\mathbf{s}') \rangle = (2\pi)^2 \delta_\mathrm{D}(\mathbf{s} - \mathbf{s}') \, P_\kappa(s). \qquad (2.18)$$

The time dependence in Eq(2.17) stands for the growth of structures. The jump from the 3-D wave vector $\mathbf{k}$ to the 2-D angular wave vector $\mathbf{s}$ is done by integrating along the line of sight, using the Limber approximation (Limber, 1954). To simplify Eq(2.15), it can be written as $\kappa(\boldsymbol{\theta}) = \int \mathrm{d}w \, q(w) \, \delta(f_K(w)\boldsymbol{\theta}, w)$. In real space, the convergence correlation function $\xi_\kappa(\Delta\boldsymbol{\theta}) = \langle \kappa(\boldsymbol{\theta})\kappa(\boldsymbol{\theta} + \Delta\boldsymbol{\theta}) \rangle$ can be eventually computed (Kaiser 1998):

$$\langle \kappa(\boldsymbol{\theta})\kappa(\boldsymbol{\theta} + \Delta\boldsymbol{\theta}) \rangle = \int \mathrm{d}w \, q(w) \int \mathrm{d}w' \, q(w') \, \langle \delta(f_K(w)\boldsymbol{\theta}, w)\delta(f_K(w')(\boldsymbol{\theta} + \Delta\boldsymbol{\theta}), w') \rangle$$

$$\simeq \int \mathrm{d}w \, q^2(w) \int \mathrm{d}w' \, \langle \delta(f_K(w)\boldsymbol{\theta}, w)\delta(f_K(w')(\boldsymbol{\theta} + \Delta\boldsymbol{\theta}), w') \rangle, \quad (2.19)$$

assuming that the selection function $q(w)$ does not vary across the largest fluctuations of the density and that the fluctuations are much smaller than the distance of the sources. In order to express all cosmic shear 2-points statistics, we are in fact interested in the convergence power spectrum $P_\kappa(s)$:

$$P_\kappa(s) = \int d\boldsymbol{\theta}\, \xi_\kappa(\boldsymbol{\theta})\, e^{-i\mathbf{s}\cdot\boldsymbol{\theta}}. \tag{2.20}$$

The density contrast $\delta(f_K(w)\boldsymbol{\theta}, w) = \delta(\mathbf{r})$ can be expressed in Fourier space:

$$\delta(\mathbf{r}) = \int \frac{d\mathbf{k}}{(2\pi)^3}\, e^{-i\mathbf{k}\cdot\mathbf{r}}\, \tilde{\delta}(\mathbf{k}, w) = \int \frac{d\mathbf{k}}{(2\pi)^3}\, e^{-i\mathbf{k}_\perp\cdot\boldsymbol{\theta}\, f_K(w)}\, e^{-i\, k_3 w}\, D_1^{(+)}(w)\, \tilde{\delta}(\mathbf{k}), \tag{2.21}$$

where $D_1^{(+)}(w)$ is the linear structure growth factor (see the next section *non-linear power spectrum*), and $\mathbf{k} = (\mathbf{k}_\perp, k_3)$, $\mathbf{k}_\perp$ is the wave-vector perpendicular to the line of sight. From this equation and Eq(2.17), one can express the density correlation function appearing in Eq(2.19):

$$\langle \delta(\mathbf{r})\delta^\star(\mathbf{r}') \rangle = \int d\mathbf{k}\, e^{-i\mathbf{k}_\perp\cdot\boldsymbol{\theta}\, f_K(w)}\, e^{i\mathbf{k}_\perp\cdot(\boldsymbol{\theta}+\Delta\boldsymbol{\theta})\, f_K(w')}$$
$$\times\, e^{-i\, k_3(w-w')}\, D_1^{(+)}(w)D_1^{(+)}(w')\, P_{3D}(k). \tag{2.22}$$

When, as in our case, the small angle approximation is valid ($|\Delta\boldsymbol{\theta}| \leqslant 1-2$ degrees), the transverse wave-vector $\mathbf{k}_\perp$ carries most of the power at $|\mathbf{k}|$; that is $P_{3D}(k) \simeq P_{3D}(k_\perp)$ (Peebles 1980). The k_3 integration then gives a Dirac delta function $\delta_D(w - w')$. If we perform the variable change $\mathbf{k}_\perp\, f_K(w) = \mathbf{s}$ the convergence power spectrum becomes:

$$P_\kappa(s) = \int dw\, \frac{q^2(w)}{f_K^2(w)} \left[D_1^{(+)}(w) \right]^2 P_{3D}\left(\frac{s}{f_K(w)} \right). \tag{2.23}$$

Back to the notations of Eq(2.15), the convergence power spectrum finally writes

$$P_\kappa(s) = \frac{9}{4} \left(\frac{H_0}{c} \right)^4 \Omega_0^2 \int_0^{w_{\rm H}} dw\, \frac{g^2(w)}{a^2(w)} P_{3D}\left(\frac{s}{f_K(w)}; w \right). \tag{2.24}$$

The expression of the shear power spectrum $P_\gamma(s)$ is identical because in Fourier space, the quantities $\langle \tilde{\kappa}^2 \rangle$ and $\langle |\tilde{\gamma}|^2 \rangle$ are identical. As we shall see, this allows us to extract the convergence 2-points statistics directly from the data.
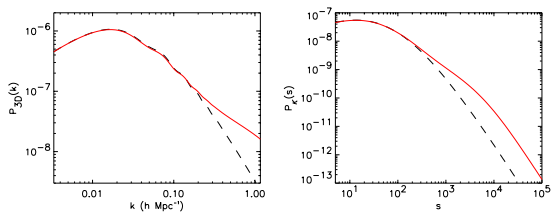
2.4. *Non-linear power spectrum*

The normalization of the mass density power spectrum P_{3D} is defined by computing the mass density variance within a sphere of 8 h^{-1}Mpc radius at redshift zero:

$$\sigma_8^2 = \langle \delta_R^2 \rangle = \frac{1}{2\pi^3} \int d\mathbf{k} P_{3D}(k, 0) |W(kR)|^2, \tag{2.25}$$

where $W(kR) = \frac{3}{(kR)^2} \left(\frac{\sin(kR)}{kR} - \cos(kR) \right)$ is the Fourier transform of the top-hat window function of radius R. The transition from the linear to the non-linear scales is identified by $\sigma_8 \sim 1$. In the linear regime, where the density contrast of the mass distribution is low ($\delta \ll 1$), the fluid equations describing the structure growth can be solved perturbatively, and one obtains for the growing mode:

$$P_{3D}(k, w) = \left[D_1^{(+)}(w) \right]^2 P_{3D}(k), \quad \text{with } D_1^{(+)}(w) = \frac{5}{2}\, \Omega_0\, H(w) \int_0^w \frac{da}{a^3\, H(a)}. \tag{2.26}$$

In the non-linear regime, the structure growth cannot be solved analytically and its

Figure 3. Left: a 3-dimensional mass power spectrum for the linear (dashed) and non-linear (solid, using Smith *et al.* 2003) regimes when baryons are included. A value of $\Omega_b = 0.05$ was used. Right: induced convergence power spectrum (Eq.2.24) for the two dynamical regimes. Other parameters are $\Omega_{\rm cdm} = 0.25, \Omega_\Lambda = 0.7, \sigma_8 = 0.9, h = 0.7, z_{\rm source} = 0.8$.

description must rely on non-linear models (Peacock & Dodds, 1996, Smith *et al.* 2003), following an original idea of Hamilton *et al.* (1991). Non-linear predictions of the matter power spectrum are performed from the knowledge of the spatial 2-points correlation function of the galaxies $\xi_2(\mathbf{r}) = \frac{V}{(2\pi)^3} \int d\mathbf{k}\, P(k)\, e^{-i\mathbf{k}\cdot\mathbf{r}}$. A measurement of $\xi_2(\mathbf{r})$ is given by the 2dF (Percival *et al.* 2001) or the SDSS surveys (Dodelson *et al.* 2002):

$$\xi_2(r) = \left(\frac{r_0}{r}\right)^\gamma, \tag{2.27}$$

with $r_0 = 4.3 \pm 0.3\ h^{-1}$Mpc and $\gamma = 1.71 \pm 0.06$. The stable clustering hypothesis stipulates that at very small scales (strong non-linear regime), the internal profile of clusters of galaxies remain constant with time for any cosmological model, and that the cluster distribution is driven by the cosmic expansion. This means that the correlation function is fixed in proper coordinates, but its amplitude evolves as a volume effect like $(1+z)^{-3}$. At large scale (linear regime), the correlation function follows the perturbation theory. Since the correlation function $\xi_2(r)$ behaves like $r^{-\gamma}$ for any cosmological model, we therefore have the two following limiting cases (Peacock 1999):
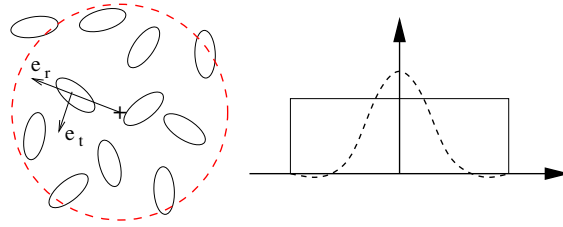
$$\xi_2(r,z) \propto (1+z)^\gamma (1+z)^{-3} \quad {\rm non-linear} \quad ; \quad \xi_2(r,z) \propto \left[D_1^{(+)}(w)\right]^2 \quad {\rm linear} \tag{2.28}$$

A mapping from the linear to the non-linear scale has been conjectured (Hamilton *et al.* 1991, Peacock & Dodds 1996, Smith *et al.* 2003), and calibrated using N-body simulation. The transition from linear to non-linear scales is described by a few slowly varying functions that depend on cosmological parameters. The same argument applies to the 3-D power spectrum, which is needed for cosmic shear predictions down to small scales (Eq.2.24) (Peacock & Dodds 1994). Figure 3 is an example of 3-dimensional and convergence power spectra in the linear and non-linear regimes. A fair amount of baryons was included (using CAMB, Lewis *et al.* 2002), in order to show that the baryon oscillations, which are clearly visible on the 3D spectrum, are severely diluted in the projected spectrum.

2.5. *2-points statistics*

In practice, the variance of the convergence (or shear, which is the same) is computed within a given smoothing window $U(\boldsymbol{\theta})$ of radius θ_c, which can be written:

$$\langle \kappa^2 \rangle_{\theta_c} = \left\langle \left(\int d^2\theta'\, U(\theta')\kappa(\theta') \right)^2 \right\rangle = \int d^2\theta'\, U(\theta') \int d^2\vartheta\, U(\vartheta) \langle \kappa(\boldsymbol{\theta}')\kappa(\boldsymbol{\vartheta}) \rangle. \tag{2.29}$$

Figure 4. In order to compute the shear variances, the galaxy ellipticities are smoothed within a window (dashed red) of fixed radius θ_c (left). The shear variance will show up as an excess of galaxy alignment with respect to random orientation. Right: profile of the two filters one usually consider, top-hat (solid line) and compensated (dashed line). Left: (e_t, e_r) axes corresponding to the local frame attached to each individual galaxy, on which the galaxy ellipticity components can be projected out to give an estimate of the tangential γ_t and radial shear γ_r.

If we express the convergence from its Fourier transform $\kappa(\boldsymbol{\theta}) = \int \mathrm{d}^2\mathbf{s} \; \tilde{\kappa}(\mathbf{s}) \; \mathrm{e}^{i\boldsymbol{\theta}\cdot\mathbf{s}}$ and using Eq(2.18), we obtain:

$$\langle\kappa^2\rangle_{\theta_c} = \int \mathrm{d}^2\theta' \, U(\theta') \int \mathrm{d}^2\vartheta \, U(\vartheta) \int \frac{\mathrm{d}^2 s}{(2\pi)^2} \, \mathrm{e}^{i\mathbf{s}\cdot(\boldsymbol{\theta}'-\boldsymbol{\vartheta})} P_\kappa(s)$$

$$= 2\pi \int_0^\infty \mathrm{d}s \, s \, P_\kappa(s) \left(\int_0^{\theta_c} \mathrm{d}\vartheta \, \vartheta \, U(\vartheta) \, \mathrm{J}_0(s\vartheta) \right)^2. \tag{2.30}$$

This expression is general, and can be applied to any smoothing window $U(\boldsymbol{\theta})$. Since $P_\gamma(s) = P_\kappa(s)$, it also expresses the shear variance $\langle\gamma^2\rangle_{\theta_c}$. As illustrated in Figure 4 , we are primarily interested in a top-hat filtering, for which,

$$\langle\gamma^2\rangle = \frac{2}{\pi} \int \mathrm{d}s \, s \, P_\kappa(s) \left[\frac{J_1(s\theta_c)}{s\theta_c} \right]^2, \tag{2.31}$$

and in the compensated filtering having $\int_0^{\theta_c} \mathrm{d}\theta \, \theta \, U(\theta) = 0$ (zero mean). The choice of $U(\theta)$ is arbitrary, provided it has a zero mean. Here we use the expression (Schneider *et al.* 1998):

$$U(\theta) = \frac{9}{\pi\theta_c^2} \left(1 - \left(\frac{\theta}{\theta_c}\right)^2 \right) \left(\frac{1}{3} - \left(\frac{\theta}{\theta_c}\right)^2 \right), \tag{2.32}$$

so the variance of the convergence with this filter is:

$$\langle M_{\mathrm{ap}}^2 \rangle = \frac{288}{\pi} \int \mathrm{d}s \, s \, P_\kappa(s) \left[\frac{J_4(s\theta_c)}{s^2\theta_c^2} \right]^2. \tag{2.33}$$

The nice feature of the compensated filter is that it is a pass-band filter, which means that the variance Eq(2.33) is a direct estimate of the convergence power spectrum in real space. Note that the power is estimated around $s \sim 5/\theta_c$. Furthermore, it can be estimated directly from the ellipticity of the galaxies, without a reconstruction of the convergence field. This remarkable property has been demonstrated by Kaiser *et al.* (1994), who have shown that Eq(2.33) can be obtained from a smoothing of the tangential component of the shear field γ_t:

$$M_{\mathrm{ap}} = \int_0^{\theta_c} \mathrm{d}\boldsymbol{\theta} \, Q(\theta) \, \gamma_t, \quad \text{where} \quad Q(\theta) = \frac{2}{\theta_c^2} \int_0^{\theta_c} \mathrm{d}\theta' \, \theta' \, U(\theta') - U(\theta). \tag{2.34}$$

The tangential shear γ_t can be obtained from the projection of the galaxy ellipticity on the local frame (Figure 4). Another 2-points statistics of interest is the shear correlation
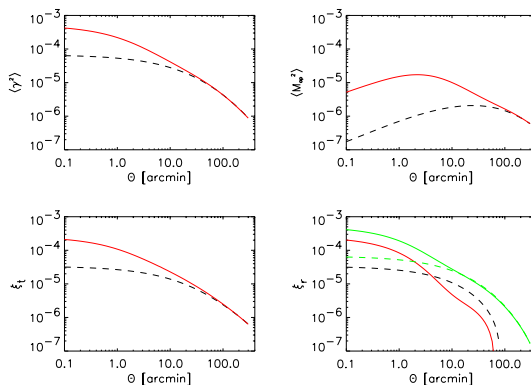
Figure 5. Lensing statistics predictions for the cosmological model used in Figure 3. Both linear (dashed) and non-linear (solid lines) regimes are represented. On the bottom-right plot, the thick dashed and solid lines are the full shear correlation function.

function $\langle \gamma \cdot \gamma \rangle_{\theta_c}$. It consists in calculating the sum of the shear product of all possible galaxy pairs separated by a distance θ_c. Using the shear field version (i.e. for $\boldsymbol{\gamma}$) of Eq(2.14), one can show that (Blandford *et al.* 1991, Miralda-Escude 1991, Kaiser 1992):

$$\langle \boldsymbol{\gamma} \cdot \boldsymbol{\gamma} \rangle_{\theta_c} = \frac{1}{2\pi} \int ds\, s\, P_\kappa(s)\, J_0(s\theta_c). \qquad (2.35)$$

One can also compute the shear correlation functions of the projected components of the shear, $\langle \gamma_t\, \gamma_t \rangle$, $\langle \gamma_r\, \gamma_r \rangle$. For symmetry reasons $\langle \gamma_t\, \gamma_r \rangle = 0$. On the other hand, the two former correlation functions are not equal, because the gravitational shear is generated by a scalar potential, implying that the projections on the local frame of the shear components are not equivalent. We can show that:

$$\langle \gamma_t\, \gamma_t \rangle_{\theta_c} = \frac{1}{4\pi} \int ds\, s\, P_\kappa(s)\, [J_0(s\theta_c) + J_4(s\theta_c)]$$

$$\langle \gamma_r\, \gamma_r \rangle_{\theta_c} = \frac{1}{4\pi} \int ds\, s\, P_\kappa(s)\, [J_0(s\theta_c) - J_4(s\theta_c)] \qquad (2.36)$$

One usually denotes $\xi_+(\theta_c) = \langle \gamma_t\, \gamma_t \rangle + \langle \gamma_r\, \gamma_r \rangle$, and $\xi_-(\theta_c) = \langle \gamma_t\, \gamma_t \rangle - \langle \gamma_r\, \gamma_r \rangle$. We have, of course, $\xi_+(\theta_c) = \langle \boldsymbol{\gamma} \cdot \boldsymbol{\gamma} \rangle_{\theta_c}$.

Figure 5 shows the linear and non-linear predictions for all the statistics defined here, for a particular cosmological model.

2.6. *Dependence on cosmological parameters*

Eq(2.14), Eq(2.24) and Eq(2.25) show that the cosmic shear signal depends primarily on the source redshift w_S, then on the mean density parameter Ω_0, and on the slope and the normalization (σ_8) of the mass power spectrum. To explore the parameter dependence of the cosmic shear signal, we assume the Cold Dark Matter model, with a power spectrum parameterized with the slope parameter Γ. We allow the four parameters $(\Omega_0, z_s, \Gamma, \sigma_8)$ to vary, and we compute the likelihood $\mathcal{L}(\Omega_0, z_s, \Gamma, \sigma_8 \mid \mathbf{d})$ of the parameters knowing the data $\mathbf{d}$. The data vector is for instance the aperture mass or any other statistic:

$$\mathcal{L} = \frac{1}{(2\pi)^{n/2} |\mathbf{S}|^{1/2}} \, \exp\left[-\frac{1}{2} (\mathbf{d} - \mathbf{s})^T \mathbf{S}^{-1} (\mathbf{d} - \mathbf{s}) \right], \qquad (2.37)$$

where $\mathbf{s}$ is the fiducial model vector and $\mathbf{S} := \langle (\mathbf{d} - \mathbf{s})^T (\mathbf{d} - \mathbf{s}) \rangle$ is the covariance matrix. Figure 6 shows the parameter dependence one expects for a survey covering 16 square
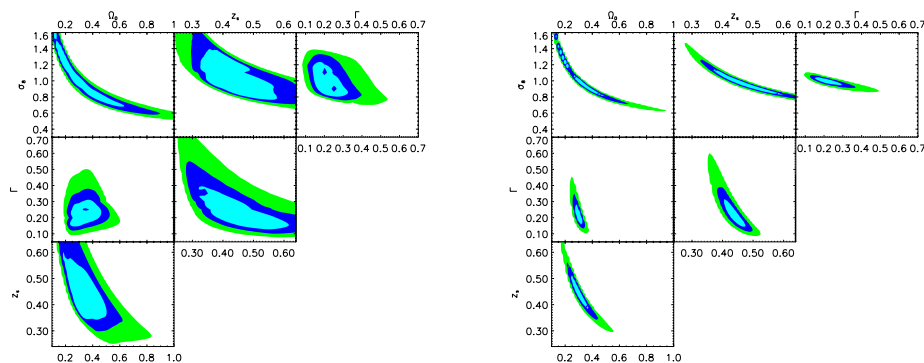
Figure 6. 1-σ, 2-σ and 3-σ confidence contours for the maximum likelihood analysis on the four parameters Ω_m, σ_8, Γ and the source redshift parameter z_s (see text). The six possible pairs of parameters are displayed. Left: On each figure, the two hidden parameters are marginalized such that $\Omega_m \in [0.2, 0.4]$, $\sigma_8 \in [0.8, 1.1]$, $\Gamma \in [0.1, 0.3]$ and $z_s \in [0.4, 0.5]$, and the cosmological constant is fixed to $\Omega_\Lambda = 1 - \Omega_m$. The model is $\Omega_m = 0.3$, $\sigma_8 = 1$, $\Gamma = 0.21$ and $z_s = 0.44$. The survey area is $A = 16 \deg^2$, the galaxy ellipticity r.m.s. is 0.3, and the correlation functions are measured in the range $0'.6 < \theta < 30'$. Right: same as left but with strong priors: the two hidden parameters as assumed to be known perfectly. These plots show the degeneracy directions among all the possible pairs of parameters obtained from Ω_m, σ_8, Γ and z_s.

degrees up to the limiting magnitude $I_{AB} = 24$, for two different choices of priors. The signal also depends on other cosmological parameters (Ω_b, Ω_Λ, Ω_ν,...), albeit to a lower extend. For precision cosmology, all parameters are relevant, but the first constraints obtained so far from cosmic shear are on the main four parameters ($\Omega_0, z_s, \Gamma, \sigma_8$).

3. Description of cosmic shear from galaxy ellipticities

3.1. *Ellipticity of the galaxies*

As mentioned in the previous Section, the cosmic shear signal is measured from the shape of the distant lensed galaxies. It is quantified from the ellipticity **e**. The raw ellipticity **e** of a galaxy is measured from the second moments I_{ij} of the surface brightness $f(\boldsymbol{\theta})$:

$$\mathbf{e} = \left(\frac{I_{11} - I_{22}}{Tr(I)}; \frac{2I_{12}}{Tr(I)} \right), \quad I_{ij} = \int \mathrm{d}^2\theta W(\theta)\theta_i\theta_j f(\boldsymbol{\theta}). \tag{3.1}$$

The window function $W(\boldsymbol{\theta})$ suppresses the noise at large distances from the object center. The cosmic shear signal can also be measured using gravitational magnification from the relative size and number count of the lensed galaxies, but this is out of the scope of this paper. Here, we only focus on the gravitational distortion effect. If one could measure the shape of the galaxies (with $W(\boldsymbol{\theta}) = 1$) perfectly without any systematics coming from the telescope tracking and the optical defects, and if the galaxies were *only* lensed, then the observed ellipticity would be related to the source ellipticity as

$$\mathbf{e}^{obs} = \frac{\mathbf{e}^{source} + \mathbf{g}}{1 + \mathbf{e}^{source} \cdot \mathbf{g}}, \tag{3.2}$$

where $\mathbf{g} = \boldsymbol{\gamma}/(1 - \kappa)$ is the reduced shear, and $\mathbf{e}^{obs}$ is the observed ellipticity, $\mathbf{e}^{source}$ is the source (unobserved) ellipticity. For nearly all cosmic shear application, the lens fields are small ($|\mathbf{g}|, \kappa \ll 1$) and the linear approximation is valid $\mathbf{e}^{obs} \simeq \mathbf{e}^{source} + \boldsymbol{\gamma}$.

Unfortunately, the ellipticity of the galaxies measured on the images are contaminated by atmospheric and instrumental distortions of the Point Spread Function (PSF) that also produce coherent non-gravitational elongation patterns, even on stars, like those on

Figure 7. This is critical issue, explains why early tentatives to measure the gravitational lensing by large scale structures failed (Valdes *et al.* 1983, Mould *et al.* 1994). Since then, various methods have been developed to correct for the non gravitational source of galaxy alignment:

• Kaiser *et al.* (1995), a method which treats the PSF convolution analytically to the first order. It is called KSB.

• Bonnet & Mellier (1995), which combines galaxy image simulation and optimal weighting of the isophotes.

• The auto-correlation function (Van Waerbeke *et al.* 1997), similar to Bonnet & Mellier (1995), but applied to the auto-correlation of the image of the galaxies to avoid some problems associated with the galaxies.

• Kuijken (1999), a method which parameterizes the PSF and the galaxies with analytical functions, and try to match the convolved profile to the data.

• Kaiser (2000), extended KSB, which circularises the PSF before the isotropic correction.

• Modified KSB (Rhodes *et al.* 2000), is the KSB approach, applied on the galaxy moments instead of the ellipticities.

• Bernstein & Jarvis (2002), is first a circularisation of the PSF, and then the convolved profile is analysed using a reduced set of orthogonal functions (Laguerre polynomials).

• The shapelets approach (Chang & Réfrégier, 2002), is a kind of Principal Components Analysis, using orthogonal Hermite polynomials functions to decompose the convolved galaxy images.

• More generally, the PCA approaches (Bertin 2001, Jarvis & Jain 2004).

The most popular, and certainly the most intensively tested (Erben *et al.* 2001, Bacon *et al.* 2001), is the KSB approach. It is a powerful correction based on the first order effect of a convolution. The idea is that we can write the first order effect of the shear and of the PSF convolution analytically as:

$$\mathbf{e}^{obs} = \mathbf{e}^{source} + \mathrm{P}_\gamma \cdot \boldsymbol{\gamma} + \mathrm{P}^{sm} \cdot \mathbf{e}^\star, \tag{3.3}$$

where P_γ and P^{sm} are tensors computed on the image (see Kaiser *et al.*, 1995), $\mathbf{e}^\star$ is the star ellipticity at the galaxy location, and $\boldsymbol{\gamma}$ is the shear signal we want to measure. Assuming that the galaxies are isotropically oriented in the source plane, we have $\langle \mathbf{e}^{source} \rangle = 0$ (which is valid even if the galaxies are intrinsically correlated), therefore the shear estimate from the measured galaxy ellipticity is given by:

$$\boldsymbol{\gamma} = \mathrm{P}_\gamma^{-1} \left(\mathbf{e}^{obs} - \mathrm{P}^{sm} \cdot \mathbf{e}^\star \right). \tag{3.4}$$

We discussed in the previous section how the shear ($\boldsymbol{\gamma}$) could be split into a radial and a tangential component γ_r and γ_t when projected onto the local frame of the aperture (Figure 4). Figure 8 (left) shows the relation between the components $\mathbf{e} = (e_1, e_2)$ of a galaxy, and its orientation. If we identify (e_1, e_2) to (e_t, e_r), we obtain the orientation in the local frame.

3.2. *E and B modes*

When the gravitational field is completely dominated by a scalar gravitational potential, only curl free modes for the shear are allowed. Any significant curl component should be interpreted as a (bad) sign of residual systematics in the data. Figure 8 (right) shows the E mode generated by over-densities (top-left) and under-densities (top-right). The two bottom curl modes are not allowed. Using the statistical properties of these patterns and the (e_t, e_r) conversion from Figure 8, it can be shown that the E modes correspond to the aperture mass $\langle M_{\mathrm{ap}}^2 \rangle$, and the B mode to the aperture mass with the galaxies 45
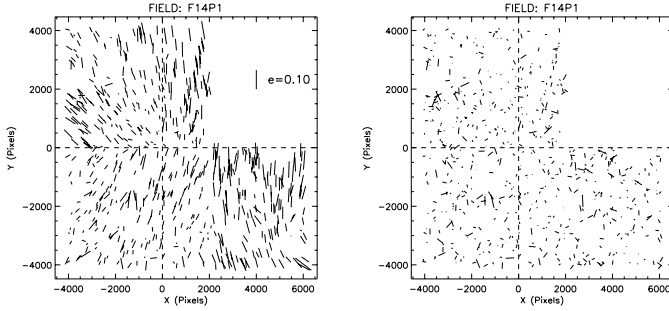
Figure 7. Uncorrected (left) and corrected(right) star ellipticities in one of cosmic shear fields.
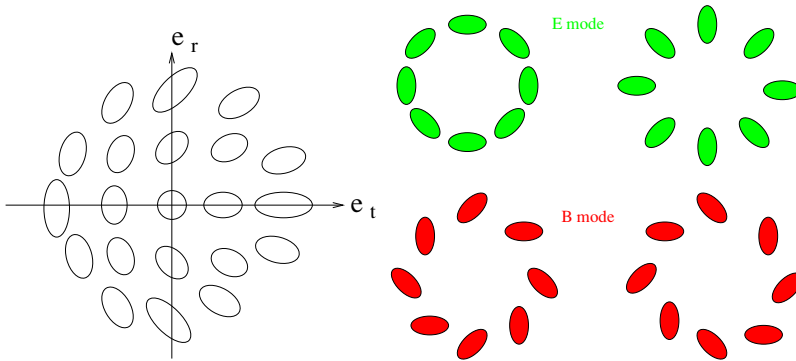
Figure 8. Left: Value of (e_t, e_r), or (e_1, e_2) in Cartesian coordinates, as a function of the shape of a galaxy with respect to the local frame attached to the galaxy. Note that the ellipticity is invariant by a rotation of π, and not 2π, this is why $e_t < 0$ and $e_r = 0$ for a vertical galaxy for instance. Right: Top patterns: shear curl free modes (E modes) allowed by gravitational lensing. Bottom patterns: curl modes (B modes) not allowed from a scalar gravitational potential. Only the E modes gives the signal of the aperture mass statistics $\langle M_{\rm ap}^2 \rangle$.

degrees rotated (such rotation corresponds to a switch $e_t \to e_r$; $e_r \to -e_t$). This is easy to understand: if there is no B mode, then switching the E into B, and B into E modes kills the signal measured with the aperture mass statistics.

3.3. *Aperture mass from the shear correlation function*

Because the E/B mode separation provides a direct and robust check of systematics error residuals, it is widely believed to be the most reliable statistics. In order to compute it, there is fortunately no need to draw a compensated filter across the data and to average the shear variance. Variances and correlation functions can be expressed one into another. The E mode aperture mass is given by

$$\langle M_{\rm ap}^2 \rangle = \pi \int_0^{2\theta_c} r dr \mathcal{W}(r)\xi_+(r) + \pi \int_0^{2\theta_c} r dr \tilde{\mathcal{W}}(r)\xi_-(r), \qquad (3.5)$$

where $\mathcal{W}(r)$ and $\tilde{\mathcal{W}}(r)$ are given in Crittenden *et al.* (2002) and Pen *et al.* (2002). The B-mode is obtained by changing the sign of the second term in Eq.(3.5). The correlation functions $\xi_+(r)$ and $\xi_-(r)$ are computed from the tangential and radial correlation functions (see Eq.2.36). In order to estimate the shear correlation functions, let $\boldsymbol{\theta}_i$ be location of the i-th galaxy, its ellipticity $\mathbf{e}(\boldsymbol{\theta}_i) = (e_1, e_2)$, and the weight w_i. The ellipticity
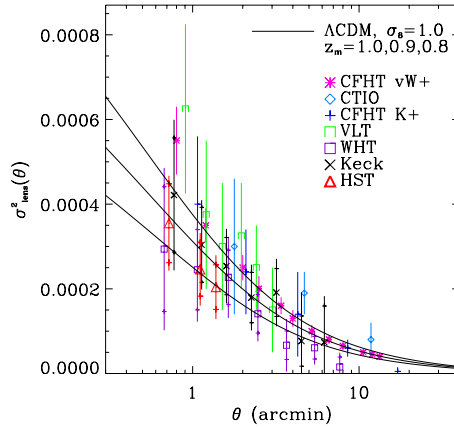
Figure 9. Recent results of top-hat shear variance measurements (Réfrégier *et al.* 2002).

is an unbiased estimate of the shear $\boldsymbol{\gamma}(\boldsymbol{\theta}_i)$. The quantity measured from the data are the binned tangential and radial shear correlation functions. They are given by a sum over galaxy pairs $(\boldsymbol{\theta}_i, \boldsymbol{\theta}_j)$

$$\xi_{tt}(r) = \frac{\displaystyle\sum_{i,j} w_i w_j e_t(\boldsymbol{\theta}_i) \cdot e_t(\boldsymbol{\theta}_j)}{\displaystyle\sum_{i,j} w_i w_j} \quad ; \; \xi_{rr}(r) = \frac{\displaystyle\sum_{i,j} w_i w_j e_r(\boldsymbol{\theta}_i) \cdot e_r(\boldsymbol{\theta}_j)}{\displaystyle\sum_{i,j} w_i w_j}, \qquad (3.6)$$

where $r = |\boldsymbol{\theta}_i - \boldsymbol{\theta}_j|$, and (e_t, e_r) are the tangential and radial ellipticities defined in the frame of the line connecting a pair of galaxies. The weights w_i are usually computed for each galaxy from the intrinsic ellipticity variance σ_e^2 and the r.m.s. of the ellipticity PSF correction σ_ϵ^2. For example, van Waerbeke *et al* (2000) measured $\sigma_e \simeq 0.4$ from their CFHT data, and defined the weights as:

$$w_i = \frac{1}{\sigma_e^2 + \sigma_\epsilon^2}. \qquad (3.7)$$

To compute σ_ϵ for each galaxy, the galaxy size-magnitude parameter space is divided into cells of constant object number. For each cell the r.m.s. of the ellipticity correction among the galaxies in the cell is computed. This choice of parameter space is motivated by the fact that the isotropic PSF correction (the P_γ term in Eq.3.3) is mainly sensitive to the size and magnitude of the galaxies.

4. Cosmology with lensing 2-pts statistics

4.1. *Measurements*

There are now several evidences of the cosmological origin of the measured signal:

(a) The consistency of the shear excess variance measured from different telescopes, at different depths and with different filters. This is summarized on Figure 9. The first detections were obtained by Bacon *et al.* 2000, Kaiser *et al.* 2000, Van Waerbeke *et al.* 2000, Wittman *et al.* 2000. Since then, several measurements have been done in different observing conditions, which are summarized in Table 1.
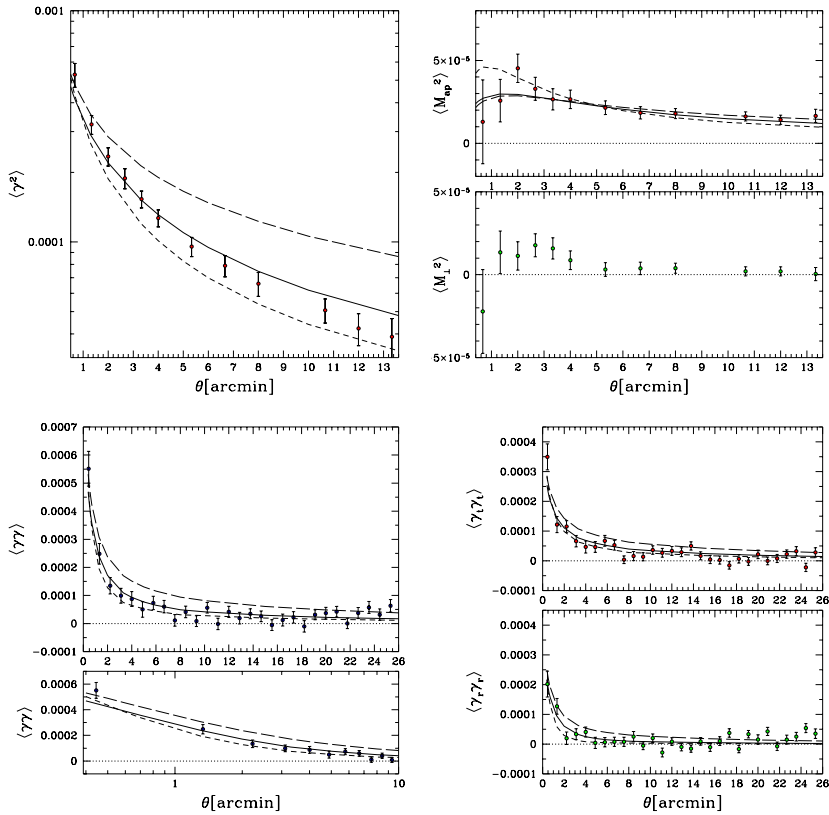
Figure 10. Measurement of all the 2-points statistics in the same survey, VIRMOS-DESCART (Van Waerbeke *et al.* 2001). Top left: top-hat variance. Top right: aperture mass E and B modes. Bottom left: full shear correlation function. Bottom right: projected shear correlation functions. survey. Right: E (top) and B (bottom) modes measured in the RCS survey. The B mode is low and the E mode compatible with the predictions for the aperture mass statistics. The lines are fiducial models which indicate the relative deviations between the statistics to the models.

(b) On a single survey, the self consistency of the different types of lensing statistics given by Eqs.(2.31,2.33,2.35,2.36). This was done on the VIRMOS-DESCART survey, and it is shown in Figure 10 (Van Waerbeke *et al.* 2001).

(c) The comparison of the E and B modes measurements (to higher accuracy than in (b)) between a deep and shallow survey for the VIRMOS-DESCART and RCS surveys (Van Waerbeke *et al.* 2002, Hoekstra *et al.* 2002). This is shown on Figure 11. More recently, the E and B modes have been also measured in other surveys (Brown *et al.* 2003, Jarvis *et al.* 2003, Hamana *et al.* 2003), which supports the cosmological origin of the signal, showing also the already small amount of residual systematics achieved with today's technology. The E and B mode measurements should now be considered as the most robust proof of the cosmological origin of the signal, and a quantitative test of systematics.

(d) The lensing signal is expected to decrease for low redshift sources, as consequence of the lower efficiency of the the gravitational distortion. It corresponds to a change in w_s in Eq(2.14), or equivalently a change in the mean source redshift with Eq(2.24). This decrease of the signal has been observed for the first time with the comparison of the E mode amplitude of the VIRMOS-DESCART survey aperture mass (see Figure 11),
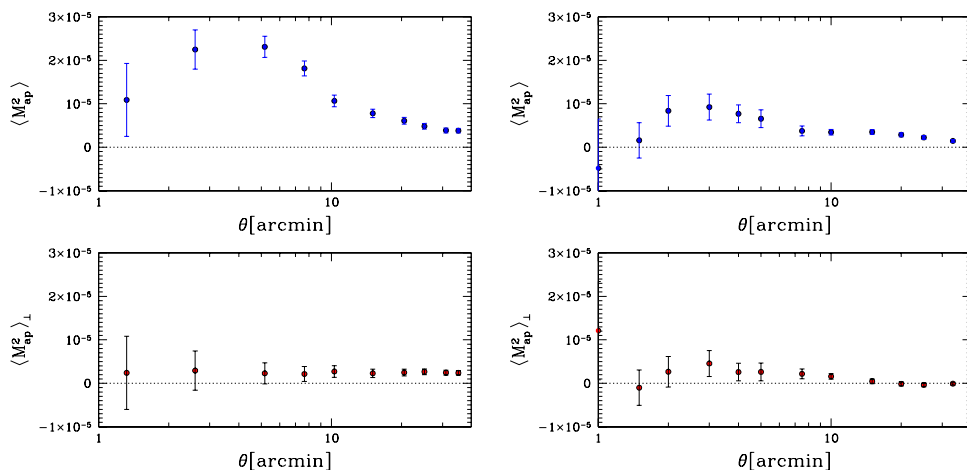
Figure 11. Left: E (top) and B (bottom) modes measured with all the most recently reduced data in the VIRMOS-DESCART survey (Van Waerbeke *et al.* 2002). Right: E (top) and B (bottom) modes measured in the RCS survey (Hoekstra *et al.* 2002). The B mode is low and the E mode compatible with the predictions for the aperture mass statistics.

which has a source mean redshift around 0.9, to the RCS which has a source mean redshift around 0.6. The expected decrease in signal amplitude is about 2, which is what is observed. This is a direct evidence of the effect of changing the redshift of the sources, a kind of 3-D cosmic shear effect.

(e) Space images provide in principle a systematics-low environment, and even if the observed areas are still smaller than ground based observations, space data provide ideal calibrations of the cosmic shear signal (Rhodes *et al.* 2001, Haemmerle *et al.* 2002, Réfrégier *et al.* 2002), which are in agreement with ground based measurements (see Figure 9, the HST points).

4.2. *Constraints*

The standard approach is to compute the likelihood of a set of n parameters $(p_1, p_2, ..., p_n)$, knowing the data vector **d**, as written in Eq(2.37). As the data vector, it is natural to choose the aperture mass variance as a function of scale $\langle M_{ap}^2 \rangle$, because the signal is split into gravitational lensing and systematics channels (the E and B modes). The B mode measures an estimate of the contamination of the E mode by systematics. The E and B modes do not equally contribute to systematic, but we know, from the measurement of the modes on the stars, that they are very similar. If the B mode is not consistent with zero, it is important to deal with it properly when estimating the cosmological parameters. Unfortunately it is not yet clear what the best approach is: some groups (Van Waerbeke *et al.* 2002, Hoekstra *et al.* 2002, Hamana *et al.* 2003) added the B mode in quadrature to the E errors, taking into account the correlation between various scales. The B mode has been subtracted first from the E mode in Hoekstra *et al.* (2002), but not in Van Waerbeke *et al.* (2002). This might probably result in a slight bias for high σ_8 values in the later. Unfortunately, it is not clear whether the B subtraction is the right correction method. Recently Jarvis *et al.* (2003) marginalised the probabilities over $E - B$ to $E + B$ taken as the signal, which is more likely to include the 'true' B mode correction one has to apply.

Minimising the B-mode contribution to cosmic shear signal is therefore a primary goal to provide reliable cosmological constraints from cosmic shear surveys. It is likely that
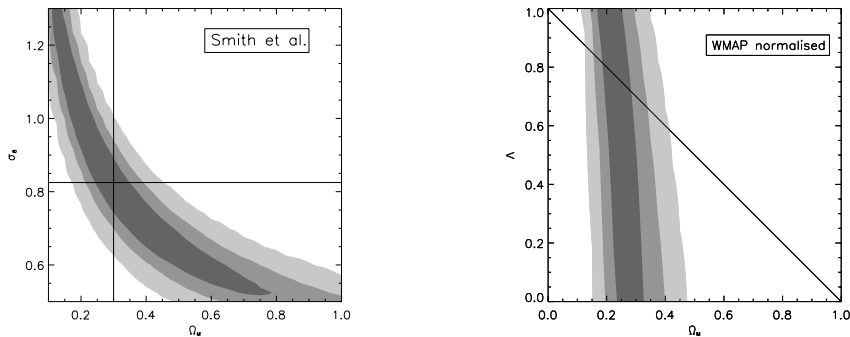
Figure 12. Constraints on cosmological parameters using the VIRMOS-DESCART data and the new PSF anisotropy correction. Left: σ_8 and Ω_M for a flat CDM Universe, adopting the non-linear power spectrum predicted by Smith *et al.* (2003). The contours include the statistical error and cosmic variance, and they correspond to the 0.68, 0.95 and 0.999 confidence levels. The solid dark vertical line indicates $\Omega = 0.3$ and the horizontal line indicates the maximum of the likelihood for σ_8 at $\Omega = 0.3$. The models are marginalised over $\Gamma \in [0.1, 0.3]$ and $z_s \in [0.4, 0.48]$. Right: VIRMOS-DESCART data constraints in the $\Lambda - \Omega_M$ plane. The models are normalised to the WMAP results ($\sigma_8 = 0.9 \pm 0.1$), and we assumed the priors $\Gamma = [0.1, 0.5]$ and $z_s = [0.4, 0.48]$. (from Van Waerbeke *et al.* 2005).

innovative PSF anisotropy correction techniques is needed to jump this barrier. In the meantime, improvements of current method can produce important results. Recently, Hoekstra (2004) and Van Waebreke *et al* (2005) made important progress using the KSB method by using new PSF interpolation model and by improving the centroid determination of galaxies. The B-mode then reduced by a factor of 5-10, leading to the most reliable cosmic shear data sets obtained at CFHT.

Figure 12 shows the joint Ω_m, σ_8 and Ω_m, Ω_Λ constraints by Van Waerbeke *et al.* (2005). They are obtained by comparing the measured lensing signal to the non-linear prediction computed numerically by Smith *et al.* (2003) which has an expected theoretical ~ 5 % r.m.s. uncertainty, not taken into account in the error contours. Therefore, the cosmological parameters cannot be known with better precision for the moment. According to the Figure 5, the transition scale between the linear and non-linear regimes is around 1 degree. The consequence is that the quoted mass normalization σ_8 is sensitive to the validity of the non-linear mapping at small scale. Jarvis *et al.* (2003) are less contaminated by this problem because they used the lensing signal from $30'$ to $100'$ to constrain the mass normalization.

Table 1 summarizes the σ_8 measurements for all the lensing surveys published so far. For simplicity it is given for $\Omega_m = 0.3$. Despite the differences among the surveys, it is worth to note that the results are all consistent within 2.5σ between the most extreme cases, when poorly known parameters are marginalised.

5. Cosmology with lensing 3-pts statistics

So far, we only discussed the 2-points statistics, but higher order statistics have been also proposed for cosmic shear (Bernardeau *et al.* 1997, Jain & Seljak 1997). If we were able to reconstruct the convergence from the shear (ellipticity) measured on the galaxies, one could for instance measure the top-hat smoothed higher order statistic easily. For

Table 1. Constraints on the power spectrum normalization "σ_8" for $\Omega_m = 0.3$ for a flat Universe. z_s is the prior used for the different surveys identified with "ID". Note that the cosmic shear results obtained by Kaiser *et al.* (2000) and Haemmerle *et al.* (2002) are not in this table because they reported a shear detection, not a σ_8 measurement.

| ID	σ_8	Statistic	Field	$m_{\rm lim}$	z_s
Maoli *et al.* 01	1.03 ± 0.05	$\langle \gamma^2 \rangle$	VLT+CTIO +WHT+CFHT	-	-
Van Waerbeke *et al.* 01	0.88 ± 0.11	$\langle \gamma^2 \rangle$, $\xi(r)$, $\langle M_{\rm ap}^2 \rangle$	CFHT 8 deg.^{2}	I=24	1.1
Rhodes *et al.* 01	$0.91^{+0.25}_{-0.29}$	$\xi(r)$	HST 0.05 deg.^{2}	I=26	0.9-1.1
Hoekstra *et al.* 02	0.81 ± 0.08	$\langle \gamma^2 \rangle$	CFHT+CTIO 24 deg.^{2}	R=24	0.55
Bacon *et al.* 03	0.97 ± 0.13	$\xi(r)$	Keck+WHT 1.6 deg.^{2}	R=25	0.7-0.9
Réfrégier *et al.* 02	0.94 ± 0.17	$\langle \gamma^2 \rangle$	HST 0.36 deg.^{2}	I=23.5	0.8-1.0
Van Waerbeke *et al.* 02	0.94 ± 0.12	$\langle M_{\rm ap}^2 \rangle$	CFHT 12 deg.^{2}	I=24	0.78-1.08
Hoekstra *et al.* 02	$0.91^{+0.05}_{-0.12}$	$\langle \gamma^2 \rangle$, $\xi(r)$ $\langle M_{\rm ap}^2 \rangle$	CFHT+CTIO 53 deg.^{2}	R=24	0.54-0.66
Brown *et al.* 03	0.74 ± 0.09	$\langle \gamma^2 \rangle$, $\xi(r)$	ESO 1.25 sq.deg.	R=25.5	0.8-0.9
Hamana *et al.* 03	$(2\sigma)0.69^{+0.35}_{-0.25}$	$\langle M_{\rm ap}^2 \rangle$, $\xi(r)$	Subaru 2.1 sq.deg.	R=26	0.8-1.4
Jarvis *et al.* 03	$(2\sigma)0.71^{+0.12}_{-0.16}$	$\langle \gamma^2 \rangle$, $\xi(r)$, $\langle M_{\rm ap}^2 \rangle$	CTIO 75 deg.^{2}	R=23	0.66
Massey *et al.* 04b	1.09 ± 0.12	$\xi(r)$	WHT 4. deg.^{2}	R=23.5	0.74-0.86
Heymans *et al.* 04	0.68 ± 0.12	$\langle \gamma^2 \rangle$, $\xi(r)$,	HST 0.22 deg.^{2}	V=27	1.1
Van Waerbeke *et al.* 05	0.83 ± 0.07	$\langle \gamma^2 \rangle$, $\xi(r)$ $\langle M_{\rm ap}^2 \rangle$	CFHT 12 deg.^{2}	I=24	0.8-1.0

instance, the skewness of the convergence, which is defined as

$$S_3(\kappa) = \frac{\langle \kappa^3 \rangle}{\langle \kappa^2 \rangle^2}, \tag{5.1}$$

is of great interest because this suited ratio of moments makes this statistic nearly independent of the normalization and shape of the power spectrum (Bernardeau *et al.* 1997). A pedagogical way to compare the second and third moments is to compute $\langle \kappa^2 \rangle$ and $S_3(\kappa)$ in the perturbation theory, and with a power law power spectrum. In that case, one finds

$$\sigma_\kappa \approx 0.01 \; \sigma_8 \; \Omega_0^{0.8} \; \left(\frac{\theta_0}{1 {\rm deg.}} \right)^{-(n+2)/2} z_s^{0.75}, \quad {\rm and} \quad s_3 \sim \frac{\langle \kappa^3 \rangle}{\langle \kappa^2 \rangle^2} \approx 40 \; \Omega_0^{-0.8} \; z_s^{-1.35}. \tag{5.2}$$

These approximated relations are not valid in the real (non-linear) world, but they show that the skewness provides a direct geometrical test (dependence on Ω_0), as long as we know the redshift of the sources z_s. Combined with the second order moment, the
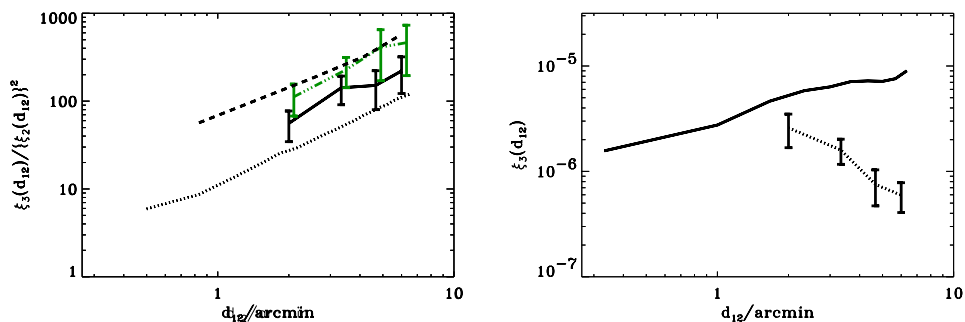
Figure 13. On the left, results for $\overline{\xi_3}(d_{12})/\overline{\xi_2}(d_{12})^2$ for the VIRMOS-DESCART survey (dot-dashed lines: $E - B$ mode for the 2-points function, solid line: $E + B$ mode for the 2-points function). This is compared to τCDM and OCDM results (dotted and dashed lines respectively). Right plot: dashed line is $\overline{\xi_3}(d_{12})$ for the VIRMOS-DESCART survey, compared to the same quantity measured on the stars.
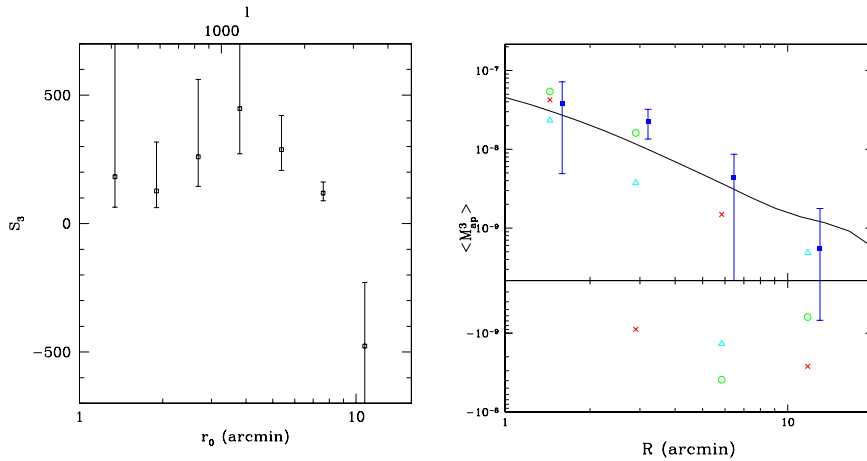
degeneracy between the power spectrum normalization and the density parameter can be broken with the cosmic shear alone.

The skewness can also be predicted in the non-linear regime, as for the 2-points statistics, using a non-linear extension of the bispectrum (Scoccimarro *et al.* 2002, Van Waerbeke *et al.* 2002). The skewness of the convergence cannot be measured on the data directly, and one needs to reconstruct κ from the shear first. This process is unfortunately sensitive to the survey geometry because the projected mass reconstruction is essentially a non-linear process. Given the complex observed field geometry generated by the masks, it is yet impossible to perform a mass reconstruction with the accuracy required to measure the cosmic shear effect. One possibility for avoiding the mass reconstruction (that is try to make the map making a local process) is to compute the third moment of the aperture mass (Schneider *et al.* 1998). In that case as well, is it sensitive to the survey geometry and it is difficult to measure an accurate third moment $\langle M_{\mathrm{ap}}^3 \rangle$.

The alternative is to measure a third moment on the shear field itself, but this cannot be done in a trivial way, since for evident symmetry reasons, any odd moment of the components of a vector field vanishes. One has to built explicitly non-trivial measures of the third moment of the shear. So far, two estimators lead to a measurement (Bernardeau *et al.* 2002 and Pen *et al.* 2002).

In Bernardeau *et al.* (2002) the idea is to identify regular shear patterns around any pair of lensed galaxies. A pair is identified by the two galaxy positions $\mathbf{x}_1$ and $\mathbf{x}_2$, and any location around the pair by $\mathbf{x}$. For a fixed pair $(\mathbf{x}_1, \mathbf{x}_2)$, we are interested in the average shear at $\mathbf{x}$. These pairs draw a typical shear pattern observed around a galaxy pair located at $(\mathbf{x}_1, \mathbf{x}_2)$. Ray tracing simulations demonstrate the stability of this shear pattern, which is almost independent on the cosmological model and the pair separation. A natural 3-points function to calculate is the average of the product of the shear correlation function $\boldsymbol{\gamma}(\mathbf{x}_1) \cdot \boldsymbol{\gamma}(\mathbf{x}_2)$ with a projection of the shear of the third galaxy $\gamma(\mathbf{x})$. The shape of the shear pattern shows that the projection is optimal when performed along the vertical axis. For a fixed pair location $(\mathbf{x}_1, \mathbf{x}_2)$, the 3-points function $\xi_3(\mathbf{x})$ and quantity we measure are respectively defined as

$$\xi_3(\mathbf{x}) = \langle \boldsymbol{\gamma}(\mathbf{x}_1) \cdot \boldsymbol{\gamma}(\mathbf{x}_2)\gamma_t(\mathbf{x}) \rangle, \quad \text{and} \quad \overline{\xi_3}(|\mathbf{x}_1 - \mathbf{x}_2|) = \int_{\mathrm{Ell.}} \frac{\mathrm{d}^2\mathbf{x}'}{V_{\mathrm{Ell.}}} \xi_3(\mathbf{x}'). \qquad (5.3)$$

Figure 14. Left : Skewness of the convergence as measured in Pen *et al.* (2002), on the VIR-MOS-DESCART survey. The overall significance of the measurement if 3.3 σ. A comparison of the signal with simulations shows that $\Omega_0 < 0.4$ at the 90% level.   Right: Skewness of the aperture mass statistic derived by Jarvis *et al* (2004) on CTIO cosmic shear data (75 deg.^{2}). The E-modes are the blue squares and mixed and B-modes are the circles, triangles, and crosses. The black curve shows the concordance ΛCDM model (From Jarvis *et al* 2004).

Figure 13 shows the result on the VIRMOS-DESCART survey. The treatment of the B mode is still uncertain, and the redshift uncertainty still too large, which makes very difficult the interpretation in terms of cosmological parameters. However Figure 13 shows that the order of magnitude, and the slope of the signal are consistent with the expectations. For instance, the signal from the stars before PSF correction is completely different in shape and amplitude.

Pen *et al.* (2002), computed the convergence aperture mass 3-points function from an integral of the shear 3-points function. This solution avoids the problem of drawing cells across a complex field geometry and presents the advantage to estimate the third moment of the convergence κ, which is the field of physical interest. Unfortunately, its measurement is still very noisy, because it uses a compensated filter that removes the low frequency modes for any target frequency (which is not the case for a top-hat filtering). The resulting skewness is shown on Figure 14 (left), and is consistent with $\Omega_0 < 0.4$ at the 90 % level.

More recently Jarvis *et al.* (2004) have also computed the three-point shear correlation function to derive skewness of the aperture mass statistic of the CTIO cosmic shear survey data (Figure 14, right panel). They found a significant positive signal and succeeded to separate E and B modes. The signal-to-noise ratio is small, but the signal is consistent with the standard Λ-CDM model.

Other approaches have been proposed (Zaldarriaga & Scoccimarro 2002, Schneider & Lombardi 2003, Takada & Jain 2003) which all deal with trying to optimize the signal-to-noise by looking for the best galaxies triangle configurations containing the highest signal. They have not yet been applied to the data.

6. Galaxy biasing

A direct byproduct of cosmic shear observations is the measure of the light/mass relation, the so-called biasing parameter b defined as the ratio of the galaxy density
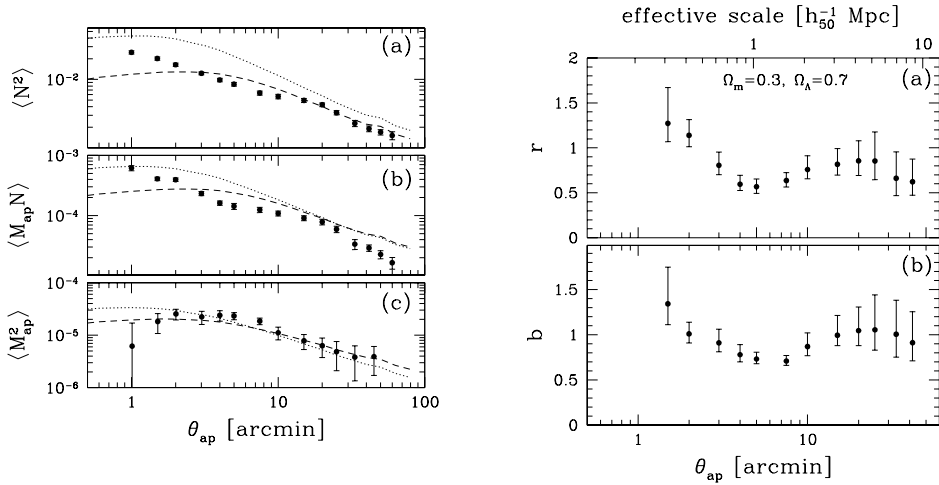
Figure 15. Left: The measurements of $\langle \mathcal{N}^2 \rangle$ (panel a), and $\langle \mathcal{N} M_{\mathrm{ap}} \rangle$ (panel b) as a function of angular scale from the RCS data. Panel c shows $\langle M_{\mathrm{ap}}^2 \rangle$ as a function of angular scale from the VIRMOS-DESCART data. The error bars for $\langle M_{\mathrm{ap}}^2 \rangle$ have been increased to account for the unknown correction for the observed "B"-mode. A few models have been plotted, assuming $b = 1$ and $r = 1$, for an OCDM cosmology (dotted line; $\Omega_m = 0.3$, $\Omega_\Lambda = 0$, $\sigma_8 = 0.9$, and $\Gamma = 0.21$) and a ΛCDM cosmology (dashed line; $\Omega_m = 0.3$, $\Omega_\Lambda = 0.7$, $\sigma_8 = 0.9$, and $\Gamma = 0.21$). Note that the points at different scales are only slightly correlated. Right: The measured value of the galaxy-mass cross correlation coefficient r as a function of scale for the ΛCDM cosmology. (b) The bias parameter b as a function of scale. The upper axis indicates the effective physical scale probed by the compensated filter at the median redshift of the lenses ($z = 0.35$).

contrast to the dark matter density contrast

$$\delta_{\mathrm{gal}} = b\, \delta_{\mathrm{mass}}. \tag{6.1}$$

This is in fact a highly simplified model, which assumes that the biasing does not vary with scale and redshift, and that the relation between mass and light is deterministic. While in the real world, none of these assumptions are correct, this model has the advantage to be tractable analytically, and to provide an average biasing estimates, which is still very useful (Van Waerbeke 1998, Schneider 1998). Nevertheless, it is possible to go beyond this simple model by combining a measurement of the dark matter clustering, galaxy clustering, and their cross-correlation by defining a biasing b and cross-correlation r such that:

$$b = \frac{\langle N_{\mathrm{ap}}^2 \rangle}{\langle M_{\mathrm{ap}}^2 \rangle}; \quad r = \frac{\langle M_{\mathrm{ap}} N_{\mathrm{ap}} \rangle}{\langle N_{\mathrm{ap}}^2 \rangle^{1/2} \langle M_{\mathrm{ap}}^2 \rangle^{1/2}}, \tag{6.2}$$

where N_{ap} is the galaxy number count density contrast smoothed with a compensated filter. Therefore, N_{ap} is similar to M_{ap}, except that it applies to the number count instead to the shear. As we discussed before, the compensated filter is a passband filter, quite narrow in Fourier space. If one chooses the number count fluctuations N_{ap} to be a foreground galaxy population with a narrow redshift distribution, then the biasing and cross-correlation b and r emerging from Eq(6.2) will be relatively localized in redshift AND wavelength. The use of well localized redshift and wavelength corresponds to a roughly fixed physical distance. Therefore we can say that, even with the simple scheme of galaxy biasing given by Eq(6.1), an estimate of b and r from Eq(6.2) is fairly local in physical scale, for the foreground galaxy population under consideration (Schneider

1998, Van Waerbeke 1998). This result has been proved to be robust against a wide range of cosmological parameters and power spectra (Van Waerbeke 1998).

This idea has been applied for the first time in the RCS data (Hoekstra *et al.* 2001). Unfortunately, this survey is not deep enough to provide an accurate measure of the dark matter clustering that could allow to separate b and r. Instead, the authors measured the ratio $b/r = 1.05^{+0.12}_{-0.10}$ for the favored ΛCDM model ($\Omega_0 = 0.3$ and $\Omega_\Lambda = 0.7$). On the other hand, a combination of deep and shallow survey could help to measure the bias and the cross-correlation independently. This was done by combining the RCS and VIRMOS-DESCART surveys (Hoekstra *et al.*, 2002). RCS is a wide shallow survey with a mean source redshift of ~ 0.6, and VIRMOS-DESCART is a deep survey with a mean source redshift ~ 0.9. By selecting the foreground population with a median redshift ~ 0.35 on the RCS survey, the number counts $\langle N_{\rm ap}^2 \rangle$, and the cross-correlation $\langle M_{\rm ap} N_{\rm ap} \rangle$ were measured. The aperture mass $\langle M_{\rm ap}^2 \rangle$ is measured on the deep survey. Figure 15 shows the measured b and r as a function of scale (angular scales are also converted to physical scale for a given cosmological model, with the lenses at $z = 0.35$). Although a proper interpretation of the measurement requires a better knowledge of the redshift distribution and cosmological parameters, it is a direct indication of the stochasticity ($r < 1$) of the biasing at small scale, and that the biasing varies with scale as we approach the galactic scales, below $1'$. The foreground galaxies were selected in R, and it was found that $b = 0.71^{+0.06}_{-0.04}$ on a scale $1 - 2 \ h_{50}^{-1}$ Mpc, and r reaches a minimum value of $r = 0.57^{+0.08}_{-0.07}$, at $1 \ h_{50}^{-1}$ Mpc. We should note that b tends toward 1 at larger scale.

The galaxy biasing analysis is one of the most important application of weak lensing because it provides clues to understand the relations between the halo formation and the star formation history in galaxies and more generally between luminous and dark matter at all scales. While weak lensing studies with SDSS already provide interesting results on galaxy biasing at low redshift (Seljak *et al* 2004), deeper cosmic shear surveys are still limited in size and shear measurement accuracy to probe its properties at higher redshift or on a very broad angular scale range. Simon et al (2004) have recently applied the same technique as described above to GaBoDS and COMBO-17 data, while Pen *et al* (2003) used another approach based on mass reconstruction. Both found similar results as Hoekstra *et al.* (2002), but did not provide yet better cosmological information on the properties of biasing.

7. Dark matter power spectrum inversion

The central interest in cosmic shear observation is dark matter. This is probably even more important than measuring the cosmological parameters, for which we have some hope to measure them accurately in the future. One important question is then: what can we say about the dark matter distribution, provided we know all the cosmological parameters? The challenge is to map the dark matter, or at least to measure its power spectrum in three dimensions, at all scales, independently of any evolution model. This is in principle possible from a direct inversion of Eq(2.24), but there are two issues here. One is that virtually, all physical wavelengths k are projected out to give a single angular wavelength s, and with a naive deprojection, one needs some cut-off somewhere in k-space to perform the invertion. The other issue is that the 3D power spectrum evolves non-linearly with redshift in the non-linear scales, therefore how could we be independent of any modeling when inverting the 2D convergence power? The first 2D convergence power spectrum estimate was performed in Pen *et al.* (2002) on the VIRMOS-DESCART data, and in Brown *et al.* (2003) on the COMBO-17 data, but the spectrum inversion was not done.
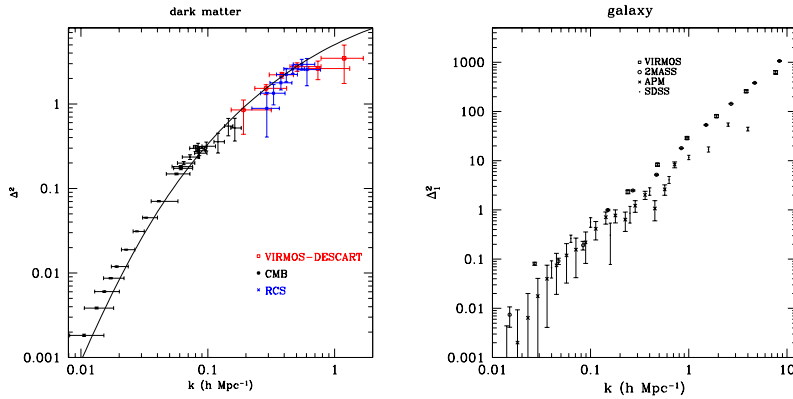
Figure 16. Left: Dark matter 3D power spectrum, deprojected from the 2D convergence power spectrum measured in the VIRMOS-DESCART survey, using SVD (Pen *et al.* 2003). The power is rescaled to $z = 0$, points are compared to the CMB (WMAP) and RCS lens survey. Right: Galaxy 3D power spectrum deprojected using the same method. For comparison, points from 2MASS, APM and SDSS are also shown.
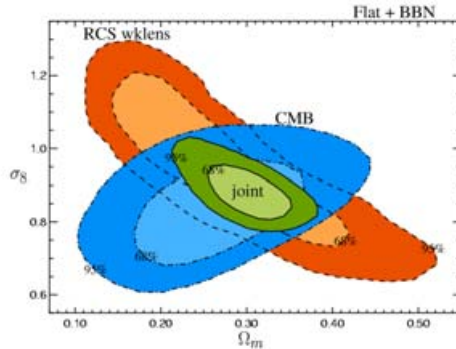
Figure 17. The two dimensional, marginalized likelihoods for the (Ω_m, σ_8) plane. The overlaid, filled contours show the 68% and 95% integration levels for the distributions. Bottom – RCS only, Middle – CMB only, Top – CMB+RCS. Courtesy Contaldi *et al.* (2003).

Pen *et al.* (2003) investigated the inversion using a singular decomposition technique, an extension of the minimum variance estimator deprojection developed in Seljak (1998). The non-linear evolution of the 3-D power spectrum was assumed to evolve *linearly* with redshift even in the non-linear regime. This hypothesis is, surprisingly, a viable assumption within the scale range of interest, and produces errors still smaller than the statistical errors. The result is shown on Figure 16 for the dark matter (top) and the galaxies (bottom). It shows a very nice agreement with the cosmic microwave background C_l's (WMAP points extrapolated at $z = 0$, see Spergel *et al.* 2003), and with clustering measurements from other galaxy surveys.

A dark matter-galaxy cross-correlation was also deprojected, allowing Pen *et al.* (2003) to estimate the 3D biasing b and matter-light correlation r. They found $b = 1.33 \pm 0.19$ and $r = 0.68 \pm 0.24$ for the *I*-selected galaxies. The bias value is slightly different than the one measured from the aperture mass on the RCS survey, but we should keep in mind that the galaxy populations are different (R compared to I selected galaxies for the RCS and VIRMOS-DESCART surveys respectively). The physical scales probed in VIRMOS-DESCART are also larger because it is a deeper survey than in RCS.

8. Join Gravitational Lensing and CMB analyses

The use of lensing with other experiments improves the accuracy of cosmological parameter measurements and eventually breaks some intrinsic degeneracies attached to each. The potential interest of combining lensing by large scale structures and cosmic microwave background experiments has been studied in Hu & Tegmark (1999). The joint study of the weak lensing RCS survey and the WMAP data performed in Contaldi *et al.* (2003) is shown on Figure 17 and illustrates the gain of this combination: it provides a direct evidence of the low value of the matter density Ω_0, which indicates a high non-zero value for the cosmological constant, independently of the supernovae result.

9. Approximations and Limitations

9.1. *Born approximation and lens-lens coupling*

The lensing theory developed in Section 1 assumes the lens can be projected onto a single plane, and therefore that the ray-tracing through a thick lens is equivalent to a thin lens appropriately weighted. Bernardeau *et al.* (1997), Schneider *et al.* (1998) or Van Waerbeke *et al.* (2002) demonstrated it is a very good approximation. If we call $\boldsymbol{\theta}$ the direction of the unperturbed ray trajectory, a ray-light passing through a first lens will be slightly deflected by an angle $\boldsymbol{\delta\theta}$, and will impact the second lens at a position angle $\boldsymbol{\theta} + \boldsymbol{\delta\theta}$ instead of $\boldsymbol{\theta}$ if the light ray were unperturbed. From a perturbative point of view, it means that expression Eq(2.11) has a correction term because the position angle to compute the lens strength is no longer $\mathbf{x} = f_K(w)\boldsymbol{\theta}$, but

$$x_i = f_K(w)\theta_i - \frac{2}{c^2} \int_0^w \mathrm{d}w' \, f_K(w - w') \, \partial_i \Phi^{(1)}(f_K(w)\boldsymbol{\theta}, w'). \qquad (9.1)$$

Eq(2.11) is therefore replaced by $\mathcal{A}_{ij}(\boldsymbol{\theta}) = \delta_{ij} + \mathcal{A}_{ij}^{(1)}(\boldsymbol{\theta}) + \mathcal{A}_{ij}^{(2)}(\boldsymbol{\theta})$ with

$$\begin{aligned}
\mathcal{A}_{ij}^{(2)}(\boldsymbol{\theta}, w) &= -\frac{2}{c^2} \int_0^w \mathrm{d}w' \, \frac{f_K(w - w')f_K(w')}{f_K(w)} \\
&\times \left[\Phi_{,ikl}(f_K(w')\boldsymbol{\theta}, w') \, x_l^{(1)}(\boldsymbol{\theta}, w')\delta_{kj} + \Phi_{,ik}(f_K(w')\boldsymbol{\theta}, w')\mathcal{A}_{kl}^{(1)}(\boldsymbol{\theta}, w') \right].
\end{aligned}$$
$$(9.2)$$

Given that the correction to the light trajectory is a second order effect in the perturbation, it is expected to become important in any high order statistics of the lensing fields. Mathematically, indeed, they have the same order than the second order dynamical correction (which is proportional to the second order gravitational potential $\Phi^{(2)}$). It turns out that the light trajectory correction is much smaller than the dynamical second order correction. The reason is that Eq(9.2) involves a second lensing efficiency factor (the ratio of angular diameter distances f_K's), which is not present in the second order dynamical correction. All comparisons of the non-linear prediction for the second and third order statistics with ray-tracing simulations show that non-linear calculations give accurate results, and that approximations are valid to better than 2 %.

9.2. *Non-linear lensing effects*

To first approximation, we consider the galaxy ellipticity an unbiased estimate of the shear. However, Eq(3.2) tells us that lensing is really non-linear. This approximation has been estimated in Barber (2002): it is negligible for sources at redshift less than $z \simeq 1$ and for scales larger than $5'$, while at smaller scale, a few percents effects could be detected. Fortunately, the use of the full non-linear lensing equation does not present any

theoretical or technical difficulties, so small scale non linear lensing effect can be easily handled. It is just usually ignored in most of the theoretical and numerical works.

9.3. *Non-linear modeling*

Ray tracing simulations demonstrate that the accuracy of non-linear predictions on the 2-points statistics is never better than 10 %, while it is never better than $\sim 20 - 30$ % for the skewness. This is a severe issue since one cannot expect to do precision cosmology if the accuracy of the model we use to extract the cosmological parameters is worse than the precision we want to reach on the cosmological parameters. Smith *et al.* (2003) proposed an improved version of non-linear modeling, which is unfortunately still insufficient. In particular, to increase the precision, we still do not know whether the baryons have to be taken into account in the modeling or not. The goal here is a modeling accurate to $1 - 3$ %, if one wants to reach the same accuracy on the cosmological parameters.

9.4. *Intrinsic alignment*

Gravitational lensing is not the only natural process which produces alignment of galaxies over large distances. Intrinsic alignment might occur from tidal fields, and produce galaxy shape correlations over cosmological distances (Croft & Metzler 2001, Catelan & Porciani 2001, Heavens *et al.* 2000, Catelan *et al.* 2001, Hatton & Ninin 2001) which should in principle split, in a predictable way, into E and B modes. There is unfortunately only partial agreement between the different predictions. Moreover, most of them stand for dark matter halos, while we are in fact observing galaxies, which should experience some alignment mixing. Concerning the dark matter halos alignment, despite the disagreement among the predictions, it is generally not believed to be higher than a 10 % contamination for a lensing survey with a mean source redshift at $z_s = 1$. An exception is Jing (2002), who suggested that intrinsic alignment could dominate the cosmic shear even in deep surveys. This possibility is already ruled out by observations. In any case, intrinsic alignment contamination *might* be an issue for studies using a single source redshift in their analysis. In the future this will not be the case since photometric redshifts will be available. The effects of intrinsic alignment will be dramatically reduced by measuring the cosmic shear correlation between distant redshift sources, instead of measuring the fully projected signal. It is then believed that intrinsic alignment should not be considered as a critical issue (Heymans & Heavens 2003, King & Schneider 2002, 2003). However, one uncertainty remains concerning the intrinsic alignment-cosmic shear correlation, which would not disapear, even with the use of photometric redshift. This residual contamination comes from the fact that intrinsic alignment must be correlated to some degree with the local tidal field, which is also correlated with the mass distribution causing the shear effect on the distant galaxies (Hirata & Seljak 2004). Therefore we expect some correlation between cosmic shear and local intrinsic alignment. The amplitude of the contamination is highly dependent on the assumed relation between the tidal field and the intrinsic alignment (where some mixing effect could be in play),and no reliable prediction have been obtained so far.

9.5. *Source clustering*

Source clustering arises because a subset of sources overlap with a subset of the lenses which are probed. There is therefore a natural bias to measure the signal preferentially in high density regions, across the overlap area. This effect gives rise to correction terms in high order statistics (Bernardeau 1998). It is easy to understand the problem if we model the source redshift distribution including a clustering term:

$$p_w(\boldsymbol{\theta}, w) = \bar{p}_w(w)(1 + \delta_{gal}(f_K(w)\boldsymbol{\theta}, w) + ...), \tag{9.3}$$

which replaces the source redshift distribution $p_w(w)$ in Eq(2.16). It is then easy to see that a density coupling occurs in Eq(2.15). According to Hamana *et al.* (2002) simulations, clustering effect it is not an issue for the 2-points statistics, but could be as high as $10 - 20$ % for the skewness of the convergence, for a narrow redshift distribution. In case of the broad redshift distribution, the effect is diluted by the bulk of non-overlapping areas. For future surveys, an accurate measure of the high order statistics will require a precise estimation of this effect. Schneider *et al.* (2003) predicted that source clustering could produce B mode in the shear maps. However, the predicted amplitude is 2 orders of magnitude and below for aperture mass scales larger than $1'$.

9.6. *PSF correction*

With the non-linear modeling of the power at small scale, this is the most serious issue concerning the cosmological interpretation of the cosmic shear signal. If we want to reach a few percents accuracy on cosmological parameters measurements, we need a PSF correction with that accuracy. So far we are able to reach 10 % precision with the KSB method for a typical signal measured on sources at $z = 1$ (Erben *et al.* 2001, Bacon *et al.* 2001, Van Waerbeke *et al.* 2002). Therefore, we still need to gain one order of magnitude. The 10 % uncertainty is an upper limit, which comes from the large B mode found in all surveys, at different scales, for probably different reasons. This upper limit is reduced if one uses the scales with very small or no B mode, but then some cosmological information is lost. So far, our understanding of the PSF variation and stability accros the CCD's and the contribution of high frequency modes is insufficient. Space data are often viewed as potentially systematics-free. This is unfortunately not true, although the PSF is certainly more stable between exposures. But one should not forget that in space, the PSF is 100 % instrumental (it is the Airy spot, which is larger than the Airy spot on the ground because space telescopes are smaller), and not anymore atmospheric. Dealing with a non circular Airy spot to correct for the galaxy shapes was not trivial for the Hubble Space Telescope for instance (Hoekstra *et al.* 1998). Qualitative estimations of shear measurement with space data done by Réfrégier *et al.* (2003) and Massey *et al.* (2004a) seem however promising.

Finally, one should emphasize that the most difficult part of the PSF correction is not the anisotropic correction, which is done quite accurately, but the isotropic correction (Erben *et al.* 2001, Hirata & Seljak 2003). The ultimate limit of PSF correction in space and on the ground is still an open question.

10. Outlook

In the WMAP (Spergel *et al.* 2003) context, the primary science goals of cosmic shear surveys must focus on the exploration of the properties of dark matter and luminous matter (see Hoektra *et al.* 2002, Pen *et al* 2002) on quasi-linear and non-linear scales where the complexity of physical processes make theoretical and numerical predictions among the most challenging tasks for the next decade. Furthermore, because cosmic shear is sensitive to the growth rate of perturbations integrated along the line-of-sight, the additional redshift information makes cosmic shear a tool to study the structure formation mechanism and the clustering history with look-back time. It is the purpose of *tomography* to study the 3D matter distribution by combining the lensing effect with the redshift information of the sources (Hu 1999, Heavens 2003). Tegmark & Zaldariaga (2002) with the RCS cosmic shear survey and Pen *et al.* (2003) with the VIRMOS-DESCART cosmic shear surveys have demonstrated that the 3-D power spectrum of the dark matter can be reconstructed. Redshift information together with galaxy clustering information provided
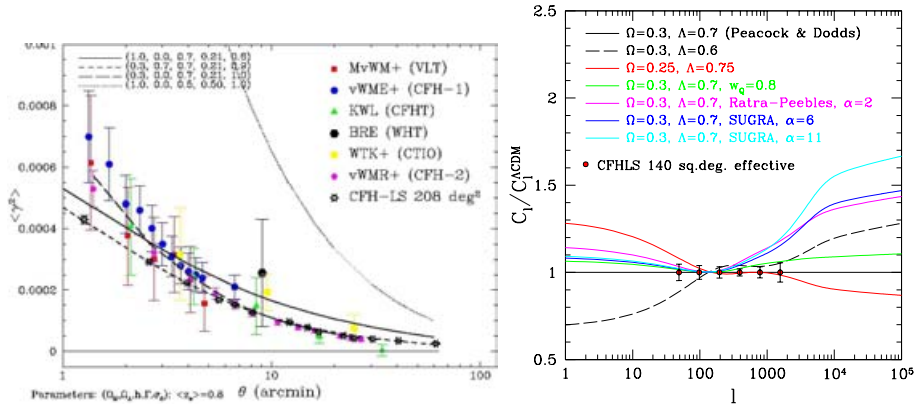
Figure 18. Left: Top hat variance of shear as function of angular scale from 6 cosmic shear surveys. The open black stars are the predictions for the CFHTLS which started by July 2003 with Megacam at CFHT. This is the expected signal from the "Wide Survey" which will cover 170 deg^2 up to $I_{AB} = 24.5$. For most points the errors are smaller than the stars. Right: Theoretical expectations on cosmological models beyond the standard model from the CFHTLS wide. The dots with error bars are the expected measurements of cosmic shear CFHTLS data. The lines shows various models discussed by Benabed & Bernardeau (2001).

also by cosmic shear surveys will also permit to decouple the geometric and pure power spectrum parts that mix together by the projected nature of the convergence field (Zhang *et al.* 2003, Hu & Jain 2004). This is a very promising approach to pin down the properties of dark energy, if any. Finally, it has been demonstrated that high order statistics are already measurable from ground based data, thus providing independent informations on cosmological models, with eventually some important degeneracies broken.

On going surveys covering hundreds of degrees will soon be in position to address relevant questions for cosmology and fundamental physics with a high degree of precision. For example, the wide CFHT Legacy Survey will cover 170 deg^2, spread over three uncorrelated fields, in 5 optical bands (and a fraction in J and K bands), and a fraction is observed also by the VMOS/VDDS spectroscopic survey (Le Fèvre *et al* 2004) and the XMM-LSS X-ray survey (Pierre *et al* 2004). Figures 18 shows some predictions of CFHTLS. The expected signal to noise of the shear variance as function of angular scale is compared to a ΛCDM cosmology. The error bars are much smaller than the VIRMOS-DESCART survey which has the same depth as CFHTLS. On Figure 18 (right), the expectations of the CFHTLS angular power spectrum are compared with the predictions of several theoretical quintessence fields models. It shows that with CFHTLS data one can already interpret cosmological data beyond standard models. Part of the CFHTLS will be also observed by the HST/ACS COSMOS Treasury Survey. It will be possible to check the reliability of ground based PSF corrected shear catalogs but also to extend the shear analysis on very small scales, down to the galactic dark halos scales. Hence, we hope to get soon a detailed view of the dark matter power spectrum and the biasing from Gpc down to kpc sales, a reliable description of individual dark halo properties (Cooray & Sheth, 2002) and on the redshift distribution of lenses and sources.

Cosmic shear data are optimized when they are used together with other surveys, like Boomerang, CBI, DASI, WMAP of Planck CMB experiments, SNIa surveys, or galaxy surveys (2dF, SDSS). The first tentative done by Contaldi, Hoekstra & Lewis (2003) and predictions provided by MCMC analysis made by Tereno *et al.* (2005) show that tight constraints can really be expected in the future. Likewise, by using cosmic magnification

instead of cosmic shear on the 100, 000 SDSS quasars, Ménard & Bartelmann (2002) have shown the cross-correlations between the foreground galaxy distribution and the quasar sample is also useful to explore the properties of the biasing and to provide similar constrains as cosmic shear. Yet, this is a widely unexplored road.

We are now entering the era of second generations of cosmic shear survey that will fully exploit the new windows opened by the first surveys. CFHTLS is one of them, but similar studies are in progress at SUBARU (Miyazaki *et al.* 2003), and NOAO, and soon at ESO, with the VST, then with VISTA, and PAN-STARRS. The third generation surveys will likely be dominated by space observations with new concepts like JDEM, SNAP , or DUNE. These projects will focus on dark energy models and, when used jointly with Planck experiments, they will be able to provide constraints on inflation scenarios as well (see Tereno *et al* 2005). We hope they will also explore our understanding of the universe far beyond the cosmological standard model to probe for instance non-standard modified gravity theories (Acquaviva *et al* 2004, Schimd *et al* 2004), and.. may be ... more exotic fields, like cosmic strings?

Acknowledgements

References

Acquaviva, V., Baccigalupi, C., , Perrotta, F. 2004, astro-ph/0409102
Bacon, D., Massey, R., Réfrégier, A., Ellis, R. 2003, *MNRAS* 344, 673
Bacon, D.J., Réfrégier, A.R., Clowe, D., Ellis, R.S. 2001, *MNRAS* 325, 1065
Bacon, D.J., Réfrégier, A.R., Ellis, R.S. 2000, *MNRAS* 318, 625
Barber, A. 2002, *MNRAS* 335, 909
Bartelmann, M., Schneider, P. 1999, *MNRAS* 345, 17
Benabed, K., Bernardeau, F. 2001, *PRD* 64,3501
Bernardeau, F. 1998, *A&A* 338, 375
Bernardeau, F., Mellier, Y., Van Waerbeke, L. 2002, *A&A* 389, L28
Bernardeau, F., Van Waerbeke, L., Mellier, Y. 1997, *A&A* 322, 1
Bernstein, G., & Jarvis, M. 2002, *AJ* 123, 583
Bertin, E. 2001, *in Mining the Sky*, Proceedings of the MPA/ESO/MPE Workshop, Garching, 31 July-4 August, 2000. Edited by A. J. Banday, S. Zaroubi, and M. Bartelmann
Blandford, R. D., Saust, A. B., Brainerd, T. G., Villumsen, J. V. 1991, *MNRAS* 251, 600
Bonnet, H., Mellier, Y. 1995, *A&A* 303, 331
Brown, M.L., Taylor, A.N., Bacon, D.J., *et al.* 2003, *MNRAS* 341, 100
Brown, M., Taylor, A. N.. Hambly, N. C.. Dye, S. 2002, *MNRAS* 333, 501
Catelan, P., Kamionkowski, M., Blandford, R. 2001, *MNRAS* 320, L7
Catelan, P., Porciani, C. 2001, *MNRAS* 323, 713
Chang, T. C., Réfrégier, A. 2002, *ApJ* 570, 447
Contaldi, C.R. , Hoekstra, H., Lewis, A. 2003, *PhRvL* 90, 1303
Cooray, A., Sheth, R. 2002, *Phys. Rep.* 372, 1
Crittenden, R., Natarajan, P., Pen, Ue-Li, Theuns, T. 2002, *ApJ* 568, 20
Croft, R., Metzler, C. 2001, *ApJ* 545, 561
Dodelson, S. *et al.* 2002, *ApJ* 572, 140
Erben T., Van Waerbeke, L., Bertin, E., Mellier, Y., Schneider, P. 2001, *A&A* 366, 717

Hamana, T., Colombi, S., Suto, Y. 2001, *A&A* 367, 18

Hamana, T., Colombi, S.T., Thion, A., Devriendt, J.E.G.T., Mellier, Y., Bernardeau, F. 2002, *MNRAS* 330, 365

Hamana, T., Miyazaki, S., Shimasaku, K., *et al.* 2003, *ApJ* 597, 98

Haemmerle H., Miralles J.M., Schneider P., Erben, T., Fosbury, R. A. E., Freudling, W., Pirzkal, N., Jain, B., White, S. D. M. 2002, *A&A* 385, 743

Hamilton, A.J.S., Kumar, P., Lu, E., Matthews, A. 1991, *ApJ* 374, L1

Hatton, S., Ninin, S. 2001, *MNRAS* 322, 576

Heavens, A. 2003, *MNRAS* 343, 1327

Heavens, A., Réfrégier, A., Heymans, C. 2000, *MNRAS* 319, 649

Heymans, C., Heavens, A. 2003, *MNRAS* 339, 711

Heymans, C., Brown, M., Barden, M., *et al.* , 2004, astro-ph/0411324

Hirata, C., Seljak, U. 2003, *MNRAS* 343, 459

Hirata, C., Seljak, U. 2004, astro-ph/0406275

Hoekstra, H., 2004 *MNRAS* 347, 133

Hoekstra, H., Franx, M., Kuijken, K., Squires, G. 1998, *ApJ* 504, 636

Hoekstra, H., Van Waerbeke, L., Gladders, M.D., Mellier, Y., Yee, H.K.C. 2002, *ApJ* 577, 604 (2002a)

Hoekstra, H., Yee, H.K.C., Gladders, M.D. 2002, *ApJ* 577, 595 (2002b)

Hoekstra, H., Yee, H.K.C., Gladders, M.D., Barrientos, L.F., Hall, P.B., Infante, L. 2002, *ApJ* 572, 55 (2002c)

Hoekstra, H., Yee, H.K. C., Gladders, M.D. 2001, *ApJ* 558, L11

Hu, W. 1999, *ApJ* 522, L21

Hu, W., Tegmark, M. 1999, *ApJ* 514, L65

Hu, W., Jain, B. 2004 *PRD* 70, 3009

Jain, B., Seljak, U. 1997, *ApJ* 484, 560

Jarvis, M., Bernstein, G. M., Fischer, P., Smith, D., Jain, B., Tyson, J. A., Wittman, D. 2003, *ApJ* 125, 1014

Jarvis, M., Bernstein, G. M., Jain, B. 2004, *MNRAS* 352, 338

Jarvis, M., Jain, B. 2004, astro-ph/0412234

Jing, Y. 2002, *MNRAS* 335, L89

Kaiser, N. 1992, *ApJ* 388, 272

Kaiser, N. 2000, *ApJ* 537, 555

Kaiser, N., Squires, G., Broadhusrt, T. 1995, *ApJ* 449, 460

Kaiser, N.,Wilson, G., Luppino, G. 2000, astro-ph/0003338

Kaiser, N., , Squires, G., Fahlman, G. & Woods, D. 1994, in *Clusters of Galaxies*, eds. F. Durret, A. Mazure & J. Tran Thanh Van, Editions Frontieres.

King, L., Schneider, P. 2002, *A&A* 396, 411

King, L., Schneider, P. 2003, *A&A* 398, 23

Kuijken, K. 1999, *A&A* 352, 355

Le Fèvre *et al.* 2004, astro-ph/0409133

Lewis, A., Challinor, A. 2002, *PRD* 66, 023531

Limber, D. 1954, *ApJ* 119, 655

Maoli, R., Van Waerbeke, L., Mellier, *et al.* 2001, *A&A* 368, 766

Massey, R., Réfrégier, A., Conselice, C., Bacon, D. 2004, *MNRAS* 348, 214 (2004a)

Massey, R., Réfrégier, A., Bacon, D., Ellis, R.S., 2004, astro-ph/0404194

Ménard, B. & Bartelmann, M. 2002, *A&A* 386, 784

Miralda-Escudé, J. 1991, *ApJ* 380, 1

Miyazaki, S., Hamana, T., Shimasaku, K., *et al.* 2003, *ApJ* 580, L97

Mould, J., Blandford, R., Villumsen, J., Brainerd, T., Smail, I., Small, T., Kells, W. 1994, *MNRAS* 271, 31

Peacock, J. 1999, *Cosmological Physics*, Cambridge University Press

Peacock, J., Dodds, S. 1994, *MNRAS* 267, 1020

Peacock, J., Dodds, S. 1996, *MNRAS* 280, 19

Peebles, P.J.E. *The Large Scale Structures of the Universe*, Princeton Series in Physics, 1980, Ed. Wightman & Anderson

Pen, U.-L., Jounghun, L., Seljak, U. 2000, *ApJ* 543, 107

Pen, U.-L., Van Waerbeke, L., Mellier, Y. 2002, *ApJ* 567, 31

Pen, U.-L., Zhang, T., Van Waerbeke, L., Mellier, Y., Zhang, P., Dubinski, J. 2003, *ApJ* 592, 664 (2003a)

Pen, U.-L., Lu, T., Van Waerbeke, L., Mellier, Y. 2003, *MNRAS* 346, 994 (2003b)

Percival, W. *et al.* 2001, *MNRAS* 327, 1297

Pierre, M. *et al.* 2004, *JCAP* 09, 11

Réfrégier, A., Bacon, D. 2003, *MNRAS* 338, 48

Réfrégier, A., Rhodes, J., Groth, E. 2002, *ApJ* 572, L131

Rhodes, J., Réfrégier, A., Groth, E. 2001, *ApJ* 552, 85

Rhodes, J., Réfrégier, A., Groth, E. 2000, *ApJ* 536, 79

Sachs, R.K. 1961, *Proc. Roy. Soc. London* A264, 309

Schimd, C., Uzan, J.-P., Riazuelo, A. 2004, 0412120

Schneider, P. 1998, *ApJ* 498, 43

Schneider, P., Lombardi, M. 2003, *A&A* 397, 809

Schneider, P., Van Waerbeke, L., Jain, B., Kruse, G. 1998, *MNRAS* 296, 873

Schneider, P., Van Waerbeke, L., Mellier, Y. 2002, *A&A* 389, 729

Scoccimarro, R., Couchman, H.M.P. 2001, *MNRAS* 325, 1312

Seljak, U. 1998, *ApJ* 503, 492

Seljak, U., Makarov, A., Mandelbaum, R., *et al.* 2004, astro-ph/0406594

Simon, P., Schneider, P., Erben, T., Schirmer, M., Wolf, C., Meisenheimer, K., 2004 astro-ph/0412139

Smith, R., Peacock, J., Jenkins, A., *et al.* 2003, *MNRAS* 341, 1311

Spergel, D., *et al.* 2003, *ApJS* 148, 175

Takada, M., Jain, B. 2003, *ApJ* 583, L49

Tegmark, M., Zaldarriaga, M. 2002, *PRD* 66, 103508

Tereno, I., Doré, O., van Waerbeke, L., Mellier, Y. *A&A* 429, 383

Valdes, F., Jarvis, J., Tyson, J. 1983, *ApJ* 271, 431

Van Waerbeke, L., Mellier, Y., Schneider, P., Fort, B., Mathez, G. 1997, *A&A* 317, 303

Van Waerbeke, L. 1998, *A&A* 334, 1

Van Waerbeke, L., Hamana, T., Scoccimarro, R., Colombi, S., Bernardeau, F. 2001, *MNRAS* 322, 918

Van Waerbeke, L., Mellier, Y., Erben, T., *et al.* 2000, *A&A* 358, 30

Van Waerbeke, L., Mellier, Y., Pelló, R., *et al.* 2002, *A&A* 393, 369

Van Waerbeke, L., Mellier, Y., Radovich, *et al.* 2001, *A&A* 374, 757

Van Waerbeke, L., Mellier, Y., Pelló, R., Pen, U.-L., McCracken, H. J., Jain, B. 2002, *A&A* 393, 369

Van Waerbeke, L., Mellier, Y., Hoekstra, H. 2005, *A&A* 429, 75

Wittman, D.M., Tyson, J.A., Kirkman, D., Dell'Antonio, I., Bernstein, G. 2000, *Nature* 405, 143

Zaldarriaga, M., Scoccimarro, R. 2003, *ApJ* 584, 559

Zhang, J., Hui, L. Stebbings, A. 2003, astro-ph/0312348